Advanced Powder Technology 33 (2022) 103628

Contents lists available at ScienceDirect

Advanced Powder Technology

journal homepage: www.elsevier.com/locate/apt

Original Research Paper

Charge source and the charging mechanism of the contact electrification of polymer powder

Masato Sakaguchi *, Masakazu Makino

Graduate School of Integrated Pharmaceutical and Nutritional Sciences, University of Shizuoka, 52 Yada, Suruga-ku, Shizuoka 422-8526, Japan

ARTICLE INFO

Article history:
Received 20 December 2021
Received in revised form 26 February 2022
Accepted 13 May 2022
Available online 30 May 2022

Keywords:
Contact-electrification
Naked-activated-charge source
Average energy level of naked-activated-charge source
Charging-mechanism
F-electron-transfer

ABSTRACT

The charge sources, as well as the charging mechanism of the contact electrification (CE) of polymers, are still debatable. Since CE is accompanied by destruction, it is considered that "hard contacting" via ball milling can induce covalent bond scission and produce naked-activated-charge sources. Regarding "soft contacting" via nano-scale sliding, which does not induce covalent bond scission, a frontier-electron, "*f-electron*," of the naked-activated-charge source is crucial to electron transfer among the naked-activated-charge sources. Here, we configure naked-activated-charge-source models, *naked-activated-mechano-anion*, and *naked-activated-mechano-cation*, which are produced by mechanical energy induced heterogeneous covalent bond scission, as well as *naked-activated-mechano-radicals* that are produced by homogeneous covalent bond scission. Regarding "soft contacting" among naked-activated-charge sources in a vacuum, *f-electron* can be transferred from a donor to an acceptor if the energy level of the donor is higher than that of the acceptor. The net amount of the normalized transferred-*f-electrons* is obtained by adopting settings in which the average energy level of the naked-activated-charge sources (as the donors) is higher than that of the sources employed as acceptors. Thus, the surfaces comprising the donors and acceptors will exhibit positive and negative net surface charges, respectively. We conclude that net surface charges depend on the average energy level of naked-activated-charge sources. Further, we observe that the alignment of polyethylene (PE)-polyvinyl chloride (PVC)-polytetrafluoroethylene (PTFE) to the average energy level is identical to that of the triboelectric series.

1. Introduction

Charging by contacting (contact electrification, CE) or rubbing (triboelectricity) is ubiquitous among polymeric materials; the phenomenon has existed since ancient times.

In conventional experiments, the amount of charge is measured by a Faraday cup (FC). However, the assignment of a charge source cannot be executed because the FC method cannot define a chemical species and its structure. Furthermore, the amount of charge is affected by many factors, including humidity, surface roughness, hot-spot temperature, oxygen, and polymer characteristics. Therefore, a charge source is still poorly defined, and the charging mechanism is still debatable.

Some studies recently reported that CE was accompanied by the fracture of polymer composites. Grzybowski and coworkers observed via Kelvin force microscopy (KFM) that the surface exhibited a uniform charge potential map before contacting a polymer; however, the surface exhibited non-uniform charge potential maps, i.e., a charge-mosaic pattern, after contacting the polymer [1]. Although KFM revealed the charge potential in the nanoscale region, it could not identify the charge source. However, their result indicated that a charge source, which was trapped on the surface, might have been produced by the contact. Employing atomic force microscopy (AFM), they further reported that the contact between polymers produced a surface charge coarsened the surface [2]. Although AFM revealed the surface roughness, it could not identify the charge source, indicating that CE induced surface coarsening (the destruction of the polymer at the surface where the charge source might have been produced and trapped). Galembeck and coworkers reported that contacting polyethylene (PE) with polytetrafluoroethylene (PTFE) revealed the non-uniform and excess charges of PE and PTFE which were positive and negative, respectively, following the triboelectric series [3]. Furthermore, they reported a review in which triboelectricity was triggered in polymers via mechanochemical wear or mass transfer

* Corresponding author.
E-mail address: sakaguchi@u-shizuoka-ken.ac.jp (M. Sakaguchi).

https://doi.org/10.1016/j.apt.2022.103628

Nomenclature

CE contact electrification
hard contacting via ball milling can induce covalent bond scission and produce naked-activated-charge sources
soft contacting via nano-scale sliding does not induce covalent bond scission, and can induce electron transfer between naked-activated-charge sources
A frontier electron "*f-electron*" of naked-activated-charge source is crucial to electron transfer between the naked-activated-charge sources
PE polyethylene
PVC polyvinyl chloride
PTFE polytetrafluoroethylene
POL = {PE, PVC, PTFE}
POL^- POL naked-activated-mechano-anion
POL^+ POL naked-activated-mechano-cation
POL POL naked-activated-mechano-radical
$POL_{ch.source,I}$ {POL^-, POL^+, $POL^\bullet$}
HOMO and *LUMO* the highest occupied molecular orbital and lowest unoccupied MO of $POL_{ch.source,i}$
$POL_{ch.source,i}${$POL^-(HOMO)$, $POL^+(HOMO)$, $POL^-(LUMO)$, $POL^+(LUMO)$, $POL^\bullet(HOMO)$, $POL^\bullet(LUMO)$} $POL_{ch.source,i}$ at the HOMO or LUMO
$E_{POLch.source,i}${$E_{POL^-(HOMO)}$, $E_{POL^+(HOMO)}$, $E_{POL^-(LUMO)}$, $E_{POL^+(LUMO)}$, $E_{POL^\bullet(HOMO)}$, $E_{POL^\bullet(LUMO)}$} the energy level of $POL_{ch.source,i}$
$I_{POLch.source,i}${$I_{POL^-(HOMO)}$, $I_{POL^+(HOMO)}$, $I_{POL^-(LUMO)}$, $I_{POL^+(LUMO)}$, $I^\bullet_{POL(HOMO)}$, $I^\bullet_{POL(LUMO)}$} the concentration of $POL_{ch.source,i}$
$^{norm}I_{POLch.source,i}$({$^{norm}I_{POL^-(HOMO)}$, $^{norm}I_{POL^+(HOMO)}$, $^{norm}I_{POL^-(LUMO)}$, $^{norm}I_{POL^+(LUMO)}$, $^{norm}I^\bullet_{POL(HOMO)}$, $^{norm}I^\bullet_{POL(LUMO)}$} the normalized $I_{POLch.source,i}$
$C^{norm}I_{POLch.source,i}${$C^{norm}I_{POL^-(HOMO)}$, $C^{norm}I_{POL^+(HOMO)}$, $C^{norm}I_{POL^-(LUMO)}$, $C^{norm}I_{POL^+(LUMO)}$, $C^{norm}I^\bullet_{POL(HOMO)}$, $C^{norm}I^\bullet_{POL(LUMO)}$} the normalized concentration of $^{norm}I_{PEch.source,i}$ with a charge sign
$^{Total,norm}SC_{hard,POLch.source,i}$ the sum of $C^{norm}I_{POLch.source,i}$s
$POL_{don,i}${$POL^-(HOMO)$, $POL^\bullet(HOMO)$, $POL^\bullet(LUMO)$, $POL^+(HOMO)$} f-electron donor of $POL_{ch.source,i}$
$POL_{acc,i}${$POL^-(LUMO)$,$POL^\bullet(LUMO)$, $POL^\bullet(HOMO)$, $POL^+(LUMO)$} f-electron acceptor of $POL_{ch.source,i}$
$E_{POLdon,i}${$E_{POL^-(HOMO)}$, $E_{POL^+(HOMO)}$, $E_{POL^\bullet(HOMO)}$, $E_{POL^\bullet(LUMO)}$} energy level of $POL_{don,i}$
$E_{POLacc,i}$ {$E_{POL^-(LUMO)}$, $E_{POL^+(LUMO)}$, $E_{POL^\bullet(LUMO)}$, $E_{POL^\bullet(HOMO)}$} energy level of $POL_{acc,i}$
$\Delta E_{POLdon,i/POLacc,i}$ energy difference between $E_{POLdon,i}$ and $E_{POLacc,i}$
$^{Fe}POL_{don,i}${$POL^-(HOMO)$, $POL^\bullet(HOMO)$, $POL^\bullet(LUMO)$} feasible f-electron donor of $POL_{don,i}$
$^{Fe}POL_{acc,i}${$POL^\bullet(LUMO)$, $POL^\bullet(HOMO)$, $POL^+(LUMO)$} feasible f-electron acceptor of $POL_{acc,i}$
$E_{FePOLdon,i}${$E_{FePOL^-(HOMO)}$, $E_{POL^\bullet(HOMO)}$, $E_{POL^\bullet(LUMO)}$} energy level of $^{Fe}POL_{don,i}$
$E_{FePOLacc,i}${$E_{POL^\bullet(LUMO)}$, $E_{POL^\bullet(HOMO)}$, $E_{POL^+(LUMO)}$} energy level of $^{Fe}POL_{acc,i}$
$^{norm}TRfE_{FePOLdon,i/FePOLacc,i}$ Concentration of normalized transferred-f-electron from $^{Fe}POL_{don,i}$ to $^{Fe}POL_{acc,i}$
$C^{norm}TRfE_{FePOLdon,i/FePOLacc,i}$ $^{norm}TRfE_{FePOLdon,i/FePOLacc,I}$ with charge sign
$^{Total,Fe}POL_{don,i}$ sum of $^{Fe}POL_{don,i}$
$^{Total,Fe}POL_{acc,i}$ sum of $^{Fe}POL_{acc,i}$
$^{Total}N_{FePOLdon,i}$ total number of $^{Fe}POL_{don,i}$
$^{Total}N_{FePOLacc,i}$ total number of $^{Fe}POL_{acc,i}$
$^{Total}N_{FePOLdon,i/FePOLacc,i}$ total number of feasible f-electron transfer pathways from $^{Fe}POL_{don,i}$ to $^{Fe}POL_{acc,i}$
$^{Total}E_{FePOLdon,i}$ total energy of $E_{FePOLdon,i}$
$^{Total}E_{FePOLacc,i}$ total energy of $E_{FePOLacc,i}$
$^{Total,norm}TRfE_{FePOLdon,i/FePOLacc,i}$ sum of $^{norm}TRfE_{FePOLdon,i/FePOLacc,i}$
$C^{Total,norm}TRfE_{FePEdon,i/FePTFEacc,i}$ the $^{Total,norm}TRfE_{FePOLdon,i/FePOLacc,i}$ with charge sign
$^{whole,Fe}POL_{don,i}$ sum of $^{Total,Fe}POL_{don,i}$ and $^{Total,Fe}POL_{acc,i}$
$^{Total}E_{whole,FePOLdon,i}$ sum of $^{Total}E_{FePOLdon,i}$ and $^{Total}E_{FePOLacc,i}$
$^{whole,Fe}POL_{acc,i}$ sum of $^{Total,Fe}POL_{don,i}$ and $^{Total,Fe}POL_{acc,i}$
$^{Total}E_{whole,FePOLacc,i}$ sum of $^{Total}E_{FePOLdon,i}$ and $^{Total}E_{FePOLacc,i}$
$^{Total}N_{whole,FePEdon,i}$ sum of $^{Total}N_{FePOLdon,i}$ and $^{Total}N_{FePOLacc,i}$
$^{Total}N_{whole,FePOLacc,i}$ sum of $^{Total}N_{FePOLdon,i}$ and $^{Total}N_{FePOLacc,i}$
$E_{Av.whole,FePOLdon,i}$ average energy of $^{whole,Fe}POL_{don,i}$
$E_{Av.whole,FePOLacc,i}$ average energy of $^{whole,Fe}POL_{acc,i}$
$\Delta C^{Net.norm}TRfE$ net amount of normalized transferred-f-electron
$^{Net.norm}SC_{soft,Av.POL}$ normalized net surface charge of POL

phenomena [4]. Moreover, Soh and coworkers reported that material transfer is key to CE [5]. These reports indicate that CE is accompanied by the destruction of polymers. Additionally, Coote et al. reported a perspective in which they outlined recent advances in the elucidation of the mechanism of CE involving insulators [6]. Whereas there are many studies on the molecular orbital calculations of "normal polymer," none has identified a charge source as the primary product of CE, thus hindering the non-disclosure of molecular orbital calculations on the primary product, and failing to clarify the charging mechanism. These limitations are due to the observation techniques, as well as the experimental conditions, which affect the charge sources. Moreover, their charging is affected by water and oxygen molecules, surface roughness, temperature, etc. Therefore, a paradigm shift in the experimental condition is necessary to reveal charge sources and their chemical structures.

Here, to reveal a charge source, mechanochemistry was applied in a vacuum via solid-state milling.

First, to reveal the molecular structure of a charge source, as well as its property, an experiment was performed in which a polymer sample was mechanically fractured in a vacuum for 21 h at 77 K via vibration glass-ball milling; therein, the glass ampoule containing the sample and balls was equipped with an electron spin resonance (ESR) spectroscopy sample tube at the top. Employing this experiment, the polymer sample was mechanically fractured in a vacuum at 77 K, producing a fine powder (notably, the glass ampoule was opened at room temperature after ball-milling, revealing that the glass balls and wall of the glass ampoule were tightly covered with the polymer powder. After removing the cover, it was confirmed that the surfaces of the glass ball and glass wall were not fractured. Put differently, no free fine powder was produced on the surfaces of glass ball and wall, although it was produced on the covered surface). Further, the fractured free powder was dropped into the ESR sample tube after ball-milling by flipping the glass ampoule upside-down in the liquid nitrogen-filled Dewar, after which it was observed in a vacuum via ESR at 77 K. The chemical structure of the powder polymer was assigned by analyzing the ESR spectra employing self-built computer program (M.S.). We have reported that the mechanical fracture of a polymer in a vacuum (77 K, 21 h) via vibration glass-ball milling induced the homogeneous scissions of the existing covalent bonds comprising a polymer main chain, as well as produced *mechano-radicals* [7–13] (regarding low-molecular-weight compounds, although powdered samples were obtained, covalent bond scission due to mechanical energy did not occur, i.e., a mechano-radical was not produced [7]). The mechano-radical was a chain-end type,

as well as a "naked" radical, which did not exhibit an interactive counter radical. Although the naked-mechano-radical was anchored to the fresh powder surface that was produced via mechanical destruction, its terminal, (the active end) protruding from the surface was highly reactive during ball milling [8–13]. This active end initiated radical polymerization in a vacuum at 77 K and produced a block copolymer, which was tethered on the surface [8–13]. These results indicated that the activation energy of the polymerization reaction, which was initiated by the naked-mechano-radical, might almost be zero. Molecular motion, e.g., that of the active end of the PE naked-mechano-radical, which was tethered to the PTFE surface in a vacuum, was extremely high, even at 77 K [8–10]. Further, the active end of the PE naked-mechano-radical at 77 K rotated freely around the carbon-carbon bond at the end of the PE main chain. These results indicated that the naked-mechano-radical, which was anchored to the surface in a vacuum, was in an isolated and activated state, also called a "*naked-activated-mechano-radical*."

Further, the 3.1×10 nm^2/ (tethered point of the block copolymer) value was estimated [9]. Namely, one naked-activated-mechano-radical occupied the nano-order area on the powder surface.

Furthermore, we previously reported that the mechanical fracture of the polymer in vacuum (77 K, 21 h) via vibration glass-ball milling induced the homogeneous and heterogeneous scission of covalent bonds comprising a polymer main chain, as well as produced a *mechano-anion* [14–19] and a *mechano-cation* [18–20] as a pair of products. Although this pair was induced by the heterogeneous covalent bond scissions of the polymer main chain, it could not be directly detected by ESR spectroscopy because the constituent species (*mechano-anion* and *a mechano-cation*) did not possess an electron spin.

Regarding the mechano-anion, we first detected it via electron spin trapping employing tetracyanoethylene (TCNE) in vacuum at 77 K [14–19]. A polymer was ball-milled in a vacuum with TCNE for 21 h at 77 K, after which a mechano-anion that had been produced via the heterogeneous covalent bond scission of the polymer main chain, donated an electron to TCNE; TCNE accepted the electron, thus producing a TCNE-anion radical (*TCNE*$^{-\bullet}$). Further, TCNE$^{-\bullet}$ was confirmed via ESR spectroscopy. Therefore, the mechano-anion was produced via ball milling in a vacuum at 77 K, after which it donated an electron to TCNE. This mechano-anion was a *naked-mechano-anion* that did not exhibit an interactive cation as a counter ion because the mechano-anion was anchored to the fresh surface in a vacuum. The *naked-mechano-anion* on the surface in vacuum at 77 K was highly reactive to TCNE; the activation energy of the reaction might almost be zero. These results indicated that the *naked-mechano-anion* on the surface in vacuum was in the activated state; put differently, this is called a "*naked-activated-mechano-anion*."

Next, a mechano-cation was produced as a paired product with the *naked-activated-mechano-anion*. However, the mechano-cation could also not be detected via ESR spectroscopy because it did not exhibit an electron spin. Thus, we first detected the mechano-cation by a mechanochemical reaction with isobutyl vinyl ether (*IBVE*; characteristic monomer for cationic polymerization) in which a poly(vinylidene fluoride)(*PVDF*) naked-mechano-cation that was anchored to PVDF in a vacuum, attracted an electron from IBVE via physical contact due to mixing; IBVE was transformed into an IBVE cation radical (*IBVE*$^{+\bullet}$), which initiated the cationic polymerization of IBVE in vacuum at 77 K to produce a poly(IBVE) homo-polymer with M_w and M_n of 6.2×10^4 and 2.3×10^4 g/mol, respectively [20]. Thus, the activation energies of the electron transfer from IBVE to the PVDF naked-mechano-cation, as well as polymerization reaction initiated by IBVE$^{+\bullet}$, might almost be approximately zero. These results indicate that the naked-mechano-cation that was anchored to the surface in vacuum was in the activated state, also called a "*naked-activated-mechano-cation*".

From the foregoing, we concluded that *naked-activated-mechano-anion* and *naked-activated-mechano-cation*, which are produced via heterogeneous covalent bond scissions due to mechanical energy, as well as *naked-activated-mechano-radicals*, which are produced by homogeneous covalent bond scissions, account for polymer charge sources in vacuum; they are anchored to the fresh powder surface produced by the mechanical destruction and isolation of the polymer on the surface in vacuum.

Second, to reveal the charging mechanism, we calculated the highest occupied molecular orbital (*HOMO*) and lowest unoccupied MO (*LUMO*) of the charge sources via using the density functional theory (*DFT*). Although we intended to calculate their HOMO and LUMO via using DFT, it was challenging because the observed polymer charge sources exhibited high molecular weights. Next, we configured model molecules of charge sources based on the following three conditions: 1. naked-activated-mechano-anion, naked-activated-mechano-cation, and naked-activated-mechano-radical as the charge sources with low molecular weights; 2. they were anchored to the surface; 3. they were isolated on the powder surface in a vacuum, i.e., the effects of solvent, oxygen, water were eliminated, and their HOMO and LUMO were calculated via DFT.

Here, we configured model molecules of the charge sources and calculated their HOMOs and LUMOs. The signs and amounts of the net charges, which were induced via feasible electron transfer from the charge source (as the donor) to another charging source (as the acceptor), were estimated employing settings in which the energy level of the donor was higher than that of the acceptor (where the activation energy of the electron transfer is zero).

2. Methods

2.1. Calculations of HOMOs and LUMOs

All the calculations reported in this paper were performed via DFT, as implemented in the Gaussian R 09W ver.7.0 program suite [21]. Becke's 3-parameter hybrid functional combined with the Le-Yang-Parr correlation functional (the B3LYP level of DFT) was utilized [22]. The input geometry-data of the models, which were submitted to the Gaussian, were prepared by a GaussView ver.5.0; to adjust the geometry, the "Clean" option in the viewer program was utilized [23]. The geometries of all the molecules were optimized to ground states in vacuum by a 6-311G(d,p) basis set and the Berny algorithm with the geometry optimization employing direct inversion in the iterative subspace (GEDIIS) in redundant internal coordinates[24]. We observed the calculated ground-state geometries of (i) naked-activated-mechano-cation, (ii) naked-activated-mechano-anion, and (iii) naked-activated-mechano-radical, and calculated the HOMO and LUMO energy levels to estimate the ease of electron transfer among these species. Regarding the radicals, since we employed an unrestricted method, a single occupied MO was divided into occupied and unoccupied ones. In this paper, the former and latter will simply be expressed as HOMO and LUMO, respectively. The calculations were performed on an HP Compaq 8100 Elite SF/CT AY032AV-A with a Windows PC.

3. Result and discussion

3.1. Model molecules of the charge source and their properties

3.1.1. Model molecules of PE charge sources and their properties

When mechanical energy, which was generated by "hard contacting" via ball milling, is loaded onto the PE model molecule

(*PE–PE*; $CH_3CH_2CH_2–CH_2CH_2CH_3$) in a vacuum at 77 K, a covalent bond comprising the main chain is heterogeneously or homogeneously cleaved, as follows:

$$PE - PE \rightarrow PE^{-}(HOMO) + PE^{+}(HOMO)\ldots\text{Heterogeneous bond scission} \quad (1)$$

$$PE - PE \rightarrow PE^{-}(LUMO) + PE^{+}(LUMO)\ldots\text{Heterogeneous bond scission} \quad (2)$$

$$PE - PE \rightarrow PE^{\bullet}(HOMO) + PE^{\bullet}(HOMO)\ldots\text{Homogenous bond scission} \quad (3)$$

$$PE - PE \rightarrow PE^{\bullet}(LUMO) + PE^{\bullet}(LUMO)\ldots\text{Homogeneous bond scission} \quad (4)$$

$PE_{ch.source,i}\{PE^{-}(HOMO),\ PE^{+}(HOMO),\ PE^{-}(LUMO),\ PE^{+}(LUMO),\ PE^{\bullet}(HOMO),\ PE^{\bullet}(LUMO)\}$ is defined as a PE charge source,i. $E_{PEch.source,i}\{E_{PE^{-}(HOMO)},\ E_{E^{+}(HOMO)},\ E_{PE^{-}(LUMO)},\ E_{PE^{+}(LUMO)},\ E_{PE\bullet(HOMO)},\ E_{PE\bullet(LUMO)}\}$ is defined as an energy level of $PE_{ch.source,i}$. Model structures of PE, $PE_{ch.source,i}$, and $E_{PEch.source,i}$ are reported in Table 1.

Further, we reported the estimation of the ionic degree of the covalent bond comprising polymer main chain by calculating the "absolute ΔMulliken atomic charge," which was defined as the difference between the Mulliken atomic charges of the two adjacent atoms comprising the covalent bond of the polymer main chain. Ionic yield of polymer increased with the increasing absolute ΔMulliken atomic charge [18].

Next, we demonstrated the distribution of the orbital coefficient of $PE_{ch.source,i}$, which was also calculated via DFT (Fig. 1). For example, regarding PE^{-}(HOMO), the distribution of the orbital coefficient at the C_3-atom (Fig. 1a) exhibited a large density lobe (Fig. 1b). Thus, the "*f-electron*," which is defined as a frontier electron on a large density lobe, for example, at the C_3-atom, can be key to the interaction as an *f-electron* donor. Moreover, regarding PE^{+}(LUMO), the distribution of the orbital coefficient at the C_3-atom (Fig. 1g) exhibited a large density lobe (Fig. 1i). Thus, an "*f-hole*," which is defined as an f-electron hole on the large density lobe, for example, at the C_3-atom, can be key to the interaction as an f-electron acceptor.

Next, the concentration of $PE_{ch.source,i}$ was estimated.

$I_{PEch.source,i}\{I_{PE^{-}(HOMO)},\ I_{PE^{+}(HOMO)},\ I_{PE^{-}(LUMO)},\ I_{PE^{+}(LUMO)},\ I^{\bullet}_{PE(HOMO)},\ I^{\bullet}_{PE(LUMO)}\}$ is defined as a concentration of $PE_{ch.source,i}$. $I_{PE^{-}(HOMO)}$ is equal to $I_{PE^{+}(HOMO)}$ because they were produced as a pair (Eq. (1)). Further, $I_{PE^{-}(LUMO)}$ is equal to $I_{PE^{+}(LUMO)}$ because they were produced as a pair (Eq. (2)). Assuming that heterogeneous scission probability of Eq. (1) is identical to that of Eq. (2), $I_{PE^{-}(HOMO)}$ is equal to the $I_{PE^{-}(LUMO)}$, and the $I_{PE^{+}(HOMO)}$ is equal to the $I_{PE^{+}(LUMO)}$. Assuming that the homogeneous scission probability of Eq. (3) is equal to that of Eq. (4), $I^{\bullet}_{PE(HOMO)}$ is equal to the $I^{\bullet}_{PE(LUMO)}$.

Further, we assume that PE^{-}(HOMO) exhibits one *f-electron* on the large density lobe, which is key to electron transfer and can release the *f-electron*. Conversely, PE^{+}(LUMO) exhibits one f-hole on the large density lobe, and it is key to the acceptance the released *f-electron*. Although $PE^{\bullet}$(HOMO) exhibits one *f-electron* or one *f-hole* on the large density lobe, $PE^{\bullet}$(LUMO) also exhibits one *f-hole* or *f-electron*.

Regarding $I_{PEch.source,i}$, ${}^{ion}I_{PEch.source,i}\{I_{PE^{-}(HOMO)},\ I_{PE^{+}(HOMO)},\ I_{PE^{-}(LUMO)},\ I_{PE^{+}(LUMO)}\}$ was defined as an ionic concentration of $PE_{ch.source,i}$. ${}^{rad}I_{PEch.source,i}\{I^{\bullet}_{PE(HOMO)},\ I^{\bullet}_{PE(LUMO)}\}$ was defined as a radical concentration of $PE_{ch.source,i}$. *Total concentration of* $PE_{ch.source,i}$ (${}^{Total}I_{PE.ch.source,i}$) was obtained by the sum of ${}^{ion}I_{PEch.source,i}$ and ${}^{rad}I_{PEch.source,i}$. Further, ${}^{ion}Y_{PEch.source,i} = {}^{ion}I_{PEch.source,i} / {}^{Total}I_{PE.ch.source,i}$, and ${}^{rad}Y_{PEch.source,i} = {}^{rad}I_{PEch.source,i} / {}^{Total}I_{PE.ch.source,i}$ were defined as ionic yield and radical yield of $PE_{ch.source,i}$, respectively. We assume that all the $PE_{ch.source,i}$ were produced by four-time scissions, and concentration of one *f-electron* was equal to that of one f-hole. Thus, ${}^{Total}I_{PE.ch.source,i}$ was given as (4×2) [f-electron]. Consequently, a ${}^{norm}I_{PEch.source,i}\{{}^{norm}I_{PE^{-}(HOMO)},\ {}^{norm}I^{+}_{PE(HOMO)},\ {}^{norm}I_{PE^{-}(LUMO)},\ {}^{norm}I^{+}_{PE(LUMO)},\ {}^{norm}I^{\bullet}_{PE(HOMO)},\ {}^{norm}I^{\bullet}_{PE(LUMO)}\}$ is defined as the normalized $I_{PEch.source,i}\{{}^{ion}Y_{PE} \times 1/(4 \times 2),\ {}^{ion}Y_{PE} \times 1/(4 \times 2),\ {}^{ion}Y_{PE} \times 1/(4 \times 2),\ {}^{ion}Y_{PE} \times 1/(4 \times 2),\ {}^{rad}Y_{PE} \times 1/(4 \times 2),\ {}^{rad}Y_{PE} \times 1/(4 \times 2)\}$. Conversely, we previously reported that the ${}^{ion}Y_{PE}$ (0.11) and ${}^{rad}Y_{PE}$ (0.89) were obtained by ball milling PE in vacuum for 21 h at 77 K [17–19]. Using ${}^{ion}Y_{PE}$ (0.11) and ${}^{rad}Y_{PE}$ (0.89), ${}^{norm}I_{PEch.source,i}$ was obtained, as presented in Table 1. Further, ${}^{C^{norm}}I_{PEch.source,i}\{C_{norm}I_{PE^{-}(HOMO)},\ {}^{C^{norm}}I_{PE^{+}(HOMO)},\ {}^{C^{norm}}I_{PE^{-}(LUMO)},\ {}^{C^{norm}}I_{PE^{+}(LUMO)},\ {}^{C^{norm}}I^{\bullet}_{PE(HOMO)},\ {}^{C^{norm}}I^{\bullet}_{PE(LUMO)}\}$ is defined as the ${}^{norm}I_{PEch.source,i}$ with a charge sign. The ${}^{C^{norm}}I_{PEch.source,i}$ value is presented in Table 1.

Contrarily, ${}^{Total,norm}SC_{hard,PEch.source,i}$ is defined as the sum of the ${}^{C^{norm}}I_{PEch.source,i}$s. Thus, ${}^{Total,norm}SC_{hard,PEch.source,i}$ is 0.00000, i.e., neutral.

3.1.2. Model molecules of PTFE charge sources and their properties

When mechanical energy owing to hard contacting via ball milling is loaded onto a PTFE model molecule (*PTFE – PTFE*; CF_3CF_2-$CF_2 - CF_2CF_2CF_3$) in a vacuum at 77 K, a covalent bond comprising the main chain is cleaved heterogeneously or homogeneously. $PTFE_{ch.source,i}\{PTFE^{-}(HOMO),\ PTFE^{+}(HOMO),\ PTFE^{-}(LUMO),\ PTFE^{+}(LUMO),\ PTFE^{\bullet}(HOMO),\ PTFE^{\bullet}(LUMO)\}$ is defined as a PTFE charge source i. $E_{PTFEch.source,i}\{E_{PTFE^{-}(HOMO)},\ E_{PTFE^{+}(HOMO)},\ E_{PTFE^{-}(LUMO)},\ E_{PTFE^{+}(LUMO)},\ E_{PTFE\bullet(HOMO)},\ E_{PTFE\bullet(LUMO)}\}$ is defined as an energy level of $PTFE_{ch.source,i}$. Model structures of PTFE, and $PTFE_{ch.source,i}$, $E_{PTFEch.source,i}$ are reported in Table 2.

Next, we demonstrated the distribution of the orbital coefficient of $PTFE_{ch.source,i}$, which was also calculated by DFT (Fig. 2). For example, regarding $PTFE^{\bullet}$(HOMO), the distribution of the orbital coefficient at the C_2-atom (Fig. 2d) revealed a large density lobe (Fig. 2e). Thus, the *f-electron* on the large density lobe at the C_2-atom can be key to the interaction as an *f-electron* donor. Conversely, regarding $PTFE^{+}$(LUMO), the distribution of the orbital coefficient at the C_2-atom (Fig. 2g) revealed large density lobe (Fig. 2i). Thus, the f-hole on the large density lobe at the C_2-atom can be key to the interaction as an *f-electron* acceptor.

Next, we estimated the concentration of $PTFE_{ch.source,i}$. All the $PTFE_{ch.source,i}$ were produced by four-time scissions. $I_{PTFEch.source,i}\{I_{PTFE^{-}(HOMO)},\ I_{PTFE^{+}(HOMO)},\ I_{PTFE^{-}(LUMO)},\ I_{PTFE^{+}(LUMO)},\ I_{PTFE\bullet(HOMO)},\ I_{PTFE\bullet(LUMO)}\}$ is defined as the concentration of $PTFE_{ch.source,i}$. Similar to the ${}^{norm}I_{PEch.source,i}$, ${}^{norm}I_{PTFEch.source,i}\{{}^{norm}I_{PTFE^{-}(HOMO)},\ {}^{norm}I_{PTFE^{+}(HOMO)},\ {}^{norm}I_{PTFE^{-}(LUMO)},\ {}^{norm}I_{PTFE^{+}(LUMO)},\ {}^{norm}I_{PTFE\bullet(HOMO)},\ {}^{norm}I_{PTFE\bullet(LUMO)}\}$ is

Table 1
Model structures of PE, $PE_{ch.source,i}$, $E_{PEch.source,i}$, ${}^{norm}I_{PEch.source,i}$, and ${}^{C^{norm}}I_{PEch.source,i}$.

$PE_{source,i}$	Model structure	$E_{PEch.source,i}$ [au]	${}^{norm}I_{PEch.source,i}$	${}^{C^{norm}}I_{PEch.source,i}$
PE^{-}(HOMO)	$CH_3CH_2CH_2–$	0.11694	0.01375	−0.01375
PE^{-}(LUMO)	$CH_3CH_2CH_2–$	0.22878	0.01375	−0.01375
$PE^{\bullet}$(HOMO)	$CH_3CH_2CH^{\bullet}_2$	−0.20503	0.11125	0.00000
$PE^{\bullet}$(LUMO)	$CH_3CH_2CH^{\bullet}_2$	−0.05110	0.11125	0.00000
PE^{+}(HOMO)	$CH_3CH_2CH^{+}_2$	−0.57603	0.01375	+0.01375
PE^{+}(LUMO)	$CH_3CH_2CH^{+}_2$	−0.40480	0.01375	+0.01375

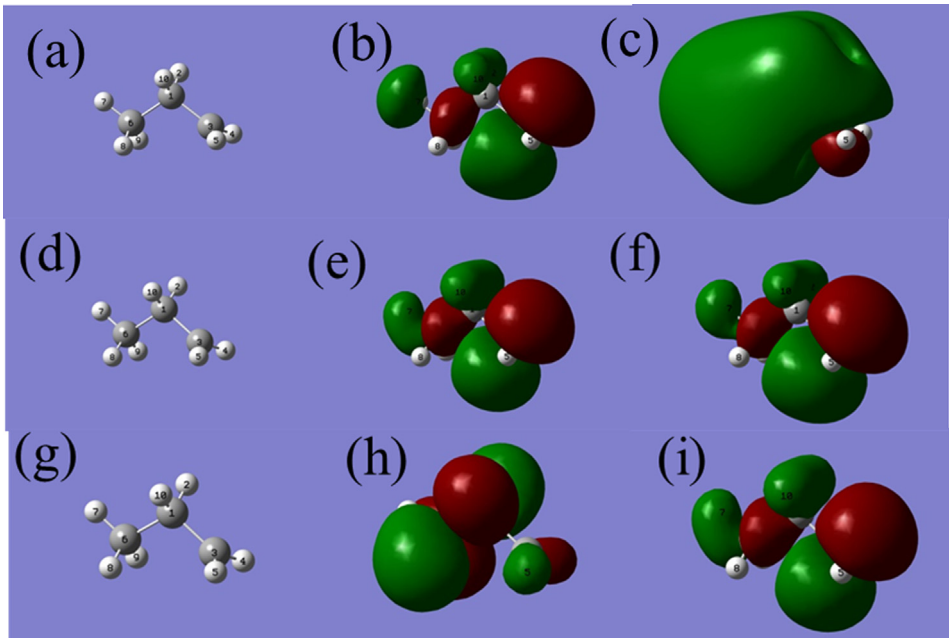

Fig. 1. Model molecule and (a) atom numbering of PE^{-}: $CH_3CH_2CH_2^{-}$. Distributions of the orbital coefficients of (b) PE^{-}(HOMO) and (c) PE^{-}(LUMO). Model molecule and (d) atom numbering of $PE^{\bullet}$: $CH_3CH_2CH_2^{\bullet}$. Distributions of the orbital coefficient of (e) $PE^{\bullet}$(HOMO) and (f) $PE^{\bullet}$(LUMO). Model molecule and (g) atom numbering of PE^{+}: $CH_3CH_2CH_2^{+}$. Distributions of the orbital coefficient of (h) PE^{+}(HOMO) and (i) PE^{+}(LUMO).

Table 2
Model structures of PTFE, $PTFE_{ch.source,i}$, $E_{PTFEch.source,i}$, $^{norm}I_{PTFEch.source,i}$, and $C^{norm}I_{PTFEch.source,i}$.

$PTFE_{ch.source,i}$	Model structure	$E_{PTFEch.source,i}$ [au]	$^{norm}I_{PTFEch.source,i}$	$C^{norm}I_{PTFEch.source,i}$
$PTFE^{-}$(HOMO)	$CF_3CF_2CF_2^{-}$	0.09858	0.02125	−0.02125
$PTFE^{-}$(LUMO)	$CF_3CF_2CF_2^{-}$	0.26369	0.02125	−0.02125
$PTFE^{\bullet}$(HOMO)	$CF_3CF_2CF_2^{\bullet}$	−0.24455	0.10375	0.00000
$PTFE^{\bullet}$(LUMO)	$CF_3CF_2CF_2^{\bullet}$	−0.09374	0.10375	0.00000
$PTFE^{+}$(HOMO)	$CF_3CF_2CF_2^{+}$	−0.61472	0.02125	+0.02125
$PTFE^{+}$(LUMO)	$CF_3CF_2CF_2^{+}$	−0.45945	0.02125	+0.02125

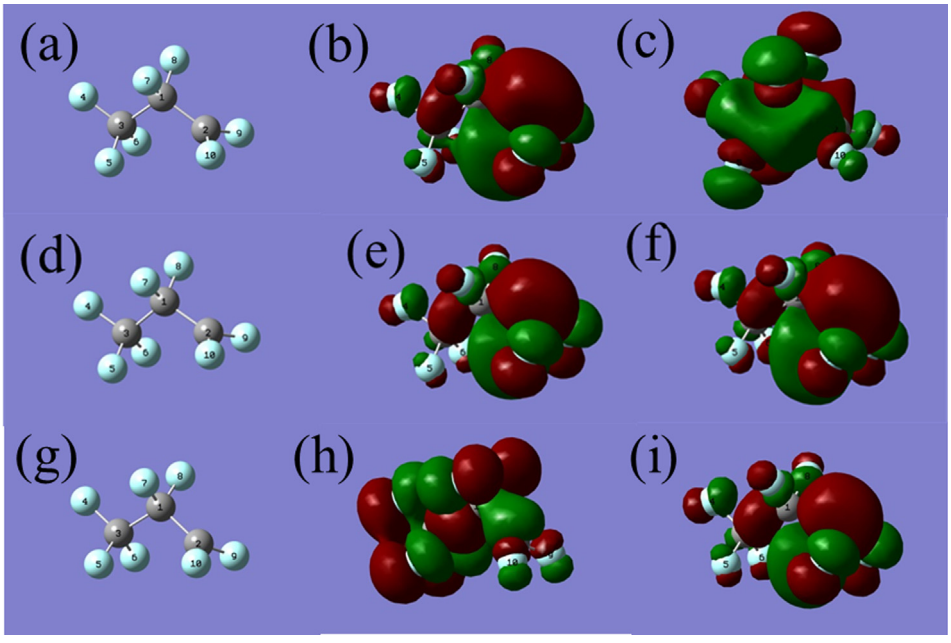

Fig. 2. Model molecule and (a) atom numbering of $PTFE^{-}$: $CF_3CF_2CF_2$-. Distributions of the orbital coefficients of (b) $PTFE^{-}$(HOMO) and (c) $PTFE^{-}$(LUMO). Model molecule and (d) atom numbering of $PTFE^{\bullet}$: $CF_3CF_2CF_2^{\bullet}$. Distributions of the orbital coefficients of (e) $PTFE^{\bullet}$(HOMO) and (f) $PTFE^{\bullet}$(LUMO). Model molecules and (g) atom numbering of $PTFE^{+}$: $CF_3CF_2CF_2^{+}$. Distributions of the orbital coefficients of (h) $PTFE^{+}$(HOMO) and (i) $PTFE^{+}$(LUMO).

defined as $I_{PTFEch.source,i}$ {$^{ion}Y_{PTFE} \times 1/(4 \times 2)$, $^{ion}Y_{PTFE} \times 1/(4 \times 2)$, $^{ion}Y_{PTFE} \times 1/(4 \times 2)$, $^{ion}Y_{PTFE} \times 1/(4 \times 2)$, $^{rad}Y_{PTFE} \times 1/(4 \times 2)$, $^{rad}Y_{PTFE} \times 1/(4 \times 2)$}. Employing $^{ion}Y_{PTFE}$(0.17) and $^{rad}Y_{PTFE}$(0.83) [17,19], $^{norm}I_{PTFEch.source,i}$ was obtained and reported in Table 2. The $C^{norm}I_{PTFEch.source,i}$ value is in Table 2.

Conversely, $^{Total,norm}SC_{hard,PTFEch.source,i}$ is defined as the sum of the $C^{norm}I_{PTFEch.source,i}$s. Thus, $^{Total,norm}SC_{hard,PTFEch.source,i}$ is 0.00000, i.e., neutral.

Next, we estimated *total f-electrons* ($^{Total}I_{f\text{-}e,PTFE}$) of $PTFE_{ch.source,i}$, which were produced by the mechanical fracture of PTFE in vacuum (77 K, 21 h). We previously reported that the concentration of PTFE mechano-radicals, which were produced by homogeneous covalent bond scissions via the vibratory ball-milling in vacuum for 21 h at 77 K was 6.8×10^{16} [spin/g], and the specific surface of the fractured PTFE was 2.1 [m^2/g] [9]. Contrarily, the concentration of the f-electrons arising from the mechano-radicals ($^{rad}I_{f\text{-}e,PTFE}$) is given as $^{rad}I_{f\text{-}e,PTFE} = {}^{Total}I_{f\text{-}e,PTFE} \times {}^{rad}Y_{PTFE}$. Thus, $^{Total}I_{f\text{-}e,PTFE} = {}^{rad}I_{f\text{-}e,PTFE} / {}^{rad}Y_{PTFE}$, Assuming that one *f-electron* is equal to one electron spin. Therefore, estimated $^{Total}I_{f\text{-}e,PTFE}$ in vacuum without the decay of the *f-electrons* is (6.8×10^{16} [spin/g]/ 0.83) / 2.1 [m^2/g] = $3.901\ 3 \times 10^{16}$ [f-electron/m^2]. In our discussion, we assumed that one *f-electron* is identical to one $PTFE_{ch.source,i}$, i.e., [one f-electron] = [one charge source]. Thus, $^{Total}I_{f\text{-}e,PTFE}$($3.9013 \times 10^{16}$ [f-electron/m^2]) is obtained as $^{Total}I_{f\text{-}e,PTFE}$ (3.9013×10^{16} [charge source/m^2]). Accordingly, each $PTFE_{ch.source,i}$ occupies the nanoscale region with 25.633 [nm^2/charge source] on the surface. We can conclude that the non-uniform charge pattern of the PTFE surface comprise charge sources in the nanoscale region.

3.1.3. Model molecules of polyvinyl chloride (PVC) charge sources and their properties

When mechanical energy due to hard contacting via ball milling is loaded onto PVC model molecule (*PVC – PVC; CH_2ClCH_2-CHCl – $CH_2CHClCH_3$*) in vacuum at 77 K, a covalent bond comprising the main chain is heterogeneously or homogeneously cleaved. *$PVC_{ch.source,i}${$PVC1^-$(HOMO), $PVC2^+$(HOMO), $PVC2^-$(HOMO), $PVC1^+$(HOMO), $PVC1^-$(LUMO), $PVC2^+$(LUMO), $PVC2^-$(LUMO), $PVC1^+$(LUMO), $PVC1^\bullet$(HOMO), $PVC2^\bullet$(HOMO), $PVC1^\bullet$(LUMO), $PVC2^\bullet$(LUMO)}* is defined as a PVC charge source i. *$E_{PVCch.source,i}${$E_{PVC1^-(HOMO)}$, $E_{PVC2^+(HOMO)}$, $E_{PVC2^-(HOMO)}$, $E_{PVC1^+(HOMO)}$, $E_{PVC1^-(LUMO)}$, $E_{PVC2^+(LUMO)}$, $E_{PVC2^-(LUMO)}$, $E_{PVC1^+(LUMO)}$, $E_{PVC1\bullet(HOMO)}$, $E_{PVC2\bullet(HOMO)}$, $E_{PVC1\bullet(LUMO)}$, $E_{PVC2\bullet(LUMO)}$}* is defined as an energy level of the $PVC_{ch.source,i}$. Model structures of PVC, $PVC_{ch.source,i}$, and $E_{PVCch.source,i}$ are reported in Table 3.

Next, the concentration of $PVC_{ch.source,i}$ was estimated. All $PVC_{ch.source,i}$ were produced by eight-time scissions. *$I_{PVCch.source,i}${$I_{PVC1^-(HOMO)}$, $I_{PVC2^-(HOMO)}$, $I_{PVC1^+(HOMO)}$, $I_{PVC2^+(HOMO)}$, $I_{PVC1^-(LUMO)}$, $I_{PVC2^-(LUMO)}$, $I_{PVC1^+(LUMO)}$, $I_{PVC2^+(LUMO)}$, $I^\bullet_{PVC1\ (HOMO)}$, $I^\bullet_{PVC2\ (HOMO)}$, $I^\bullet_{PVC1\ (LUMO)}$, $I^\bullet_{PVC2\ (LUMO)}$}* is defined as the concentration of $PVC_{ch.source,i}$. Similar to the $^{norm}I_{PEch.source,i}$, *$^{norm}I_{PVC.ch.souurce,i}${$^{norm}I_{PVC1^-(HOMO)}$, $^{norm}I_{PVC2^-(HOMO)}$, $^{norm}I_{PVC1^+(HOMO)}$, $^{norm}I_{PVC2^+(HOMO)}$, $^{norm}I_{PVC1^-(LUMO)}$, $^{norm}I_{PVC2^-(LUMO)}$, $^{norm}I_{PVC1^+(LUMO)}$, $^{norm}I_{PVC2^+(LUMO)}$, $^{norm}I^\bullet_{PVC1\ (HOMO)}$, $^{norm}I^\bullet_{PVC2\ (HOMO)}$, $^{norm}I^\bullet_{PVC1\ (LUMO)}$, $^{norm}I^\bullet_{PVC2\ (LUMO)}$}* is defined as $I_{PVCch.source,i}${$^{ion}Y_{PVC} \times 1/(8 \times 2)$, $^{ion}Y_{PVC} \times 1/(8 \times 2)$, $^{ion}Y_{PVC} \times 1/(8 \times 2)$, $^{ion}Y_{PVC} \times 1/(8 \times 2)$, $^{ion}Y_{PVC} \times 1/(8 \times 2)$, $^{ion}Y_{PVC} \times 1/(8 \times 2)$, $^{ion}Y_{PVC} \times 1/(8 \times 2)$, $^{rad}Y_{PVC} \times 1/(8 \times 2)$, $^{rad}Y_{PVC} \times 1/(8 \times 2)$, $^{rad}Y_{PVC} \times 1/(8 \times 2)$, $^{rad}Y_{PVC} \times 1/(8 \times 2)$}. Using $^{ion}Y_{PVC}$ (0.50) and $^{rad}Y_{PVC}$ (0.50) [17,19], $^{norm}I_{PVCch.source,i}$ is obtained and presented in Table 3. Further, $C^{norm}I_{PVCch.source,i}$ is listed in Table 3.

Conversely, $^{Total,norm}SC_{hard,PVCch.source,i}$ is defined as the sum of the $C^{norm}I_{PVCch.source,i}$s. Thus, $^{Total,norm}SC_{hard,PVCch.source,i}$ is 0.00000 (neutral).

3.2. CE of polymers in vacuum

We had reported that the charging of polymer might be due to the transfer of an electron from a mechano-anion to a mechano-radical based on the "electron-release potential" of the mechano-anion [17,25]. Although our study was the first to report that mechano-anion and mechano-radical correlated with CE of a polymer, the proposed mechanism was inadequate because it eliminated a mechano-cation, which was produced by heterogeneous covalent bond scission, from the reaction system. Sequentially, we proposed a charging mechanism in which charging was due to the transfer of electrons among mechano-anion, mechano-radical, and mechano-cation [26]. However, our proposed electron-transfer pathways were insufficient. Accordingly, whole feasible electron-transfer pathways could not be elucidated and the net amount of transferred electrons could not be speculated. However, there was no evidence of the correlation between charging and the covalent bond scission of polymers during the study.

Recently, although a charge source was not clarified, some studies reported [1–5] that CE was accompanied by the fracture of polymers, (detail in Section 1).

Here, we assumed the sign and net amount of the normalized transferred *f-electrons* from the charge source (donor) to another charging source (acceptor) in the settings in which the average energy level of the donors is higher than that of the acceptors (activation energy of the *f-electron* = 0.0000). (Notably, regarding the transfer of the *f-electron* from the charge source (donor) to the charge source (acceptor), we assumed that the activation energy should be zero owing to the extremely high reactivity even at 77 K, the naked structure, in vacuum isolation, and the C–C single bond at the terminal of the chain). Here, we demonstrated that the sign and net normalized surface charge depend on the average energy level of the charge sources. Further, we demonstrated that the alignment of the polymers based on the average energy level of the charge sources is identical to the alignment of the polymers from the positive charge to the negative on the triboelectric series.

Table 3
Model structures of PVC, $PVC_{ch.source,i}$, $E_{PVCch.source,i}$, $^{norm}I_{PVCch.source,i}$, and $C^{norm}I_{PVCch.source,i}$.

$PVC_{ch.source,i}$	Model structure	$E_{PVCch.source,i}$ [au]	$^{norm}I_{PVCch.source,i}$	$C^{norm}I_{PVCch.source,i}$
$PVC1^-$(HOMO)	$CH_2ClCH_2CHCl^-$	0.06700	0.03125	−0.03125
$PVC2^-$(HOMO)	$CH_3CHClCH_2^-$	0.09314	0.03125	−0.03125
$PVC1^-$(LUMO)	$CH_2ClCH_2CHCl^-$	0.19426	0.03125	−0.03125
$PVC2^-$(LUMO)	$CH_3CHClCH_2$-	0.21606	0.03125	−0.03125
$PVC1^\bullet$(HOMO)	$CH_2ClCH_2CHCl^\bullet$	−0.22376	0.03125	0.00000
$PVC2^\bullet$(HOMO)	$CH_3CHClCH^\bullet_2$	−0.22663	0.03125	0.00000
$PVC1^\bullet$(LUMO)	$CH_2ClCH_2CHCl^\bullet$	−0.08577	0.03125	0.00000
$PVC2^\bullet$(LUMO)	$CH_3CHClCH^\bullet_2$	−0.07229	0.03125	0.00000
$PVC1^+$(HOMO)	$CH_2ClCH_2CHCl^+$	−0.47085	0.03125	+0.03125
$PVC2^+$(HOMO)	$CH_3CHClCH_2^+$	−0.50460	0.03125	+0.03125
$PVC1^+$(LUMO)	$CH_2ClCH_2CHCl^+$	−0.39067	0.03125	+0.03125
$PVC2^+$(LUMO)	$CH_3CHClCH_2^+$	−0.41251	0.03125	+0.03125

3.2.1. Ce of PE and PTFE in vacuum

CE of PE and PTFE were discussed based on the transfer of the *f-electron* between $PE_{ch.source,i}$ and $PTFE_{ch.source,i}$ in a vacuum.

First, we considered the hard contact between PE and PTFE in a vacuum. $PE_{ch.source,i}$ is produced by covalent bond scission, which is induced by mechanical energy due to the hard contacting and is anchored to the surface of PE. Concurrently, $PTFE_{ch.source,i}$ is produced by covalent bond scission due to the hard contacting and is anchored to the surface of PTFE. Consequently, the PE surface exhibits a charge-mosaic pattern that is comprising a nano-scale regional charge from $PE_{ch.source,i}$; although this surface exhibits a charge-mosaic pattern, $^{Total,norm}SC_{hard,PEch.source,i}$ is 0.00000 (neutral). Although the PTFE surface also exhibits the charge-mosaic pattern comprising a nano-scale regional charge from $PTFE_{ch.source,i}$, $^{Total,norm}SC_{hard,PTFEch.source,i}$ is also 0.00000 (neutral).

Second, we considered the "*soft contacting*" between $PE_{ch.source,i}$ and $PTFE_{ch.source,i}$. Soft contacting refers to nano-scale sliding; it does not cause bond scission and can induce *f-electron* transfer between $PE_{ch.source,i}$ and $PTFE_{ch.source,i}$. The contacting combinations between $PE_{ch.source,i}$ and $PTFE_{ch.source,i}$ are considered in 32 combinations, which are divided into two categories: one category comprises 16 combinations of $PE_{don,i}$ and $PTFE_{acc,i}$, i.e., 16 pathways that might account for *f-electron* transfer from $PE_{don,i}$ to $PTFE_{acc,i}$. The other category comprises 16 combinations of $PTFE_{don,i}$ and $PE_{acc,i}$, i.e., 16 pathways that might represent an *f-electron* transfer from $PTFE_{don,i}$ to $PE_{acc,i}$. Regarding soft contacting, it was assumed that the total f-electrons of $PE_{ch.source,i}$ ($^{Total}I_{f\text{-}e,PE}$) are identical to those of $PTFE_{ch.source,i}$ ($^{Total}I_{f\text{-}e,PTFE}$), indicating that the concentrations of $PE_{ch.source,i}$ and $PTFE_{ch.source,i}$ are normalized to the products by four-time scissions.

First, we considered *f-electron* transfer from $PE_{don,i}$ to $PTFE_{acc,i}$ in a vacuum.

For example, regarding the soft contacting of PE^{-}(HOMO) with $PTFE^{\bullet}$(LUMO), the transfer an *f-electron* from PE^{-}(HOMO) (donor) to $PTFE^{\bullet}$(LUMO) (acceptor) can be executed without consuming additional energy because $\Delta E_{PE^{-}(HOMO)/PTFE^{\bullet}(LUMO),2}$ = $E_{PE^{-}(HOMO)}$ (0.11694) – $E^{\bullet}_{PTFE\ (LUMO)}$ (−0.09374) = 0.21068 > 0.00000 a.u., and the density lobes at the C_3- and C_2-atoms of PE^{-}(HOMO) (Fig. 1b) and $PTFE^{\bullet}$(LUMO) (Fig. 2f), respectively, are large. This feasible *f-electron* transfer pathway is presented in Table 4 as PE^{-}(HOMO) → $PTFE^{\bullet}$(LUMO) in the line of the pathway, Arabic numeral 2. Regarding this feasible *f-electron* transfer pathway, $^{norm}TRfE^{\bullet}_{PE^{-}(HOMO)/PTFE(LUMO),2}$ is defined as the concentration of normalized transferred f-electron from PE^{-}(HOMO) (donor) to $PTFE^{\bullet}$(LUMO) (acceptor). The values of $^{norm}TRfE_{PE^{-}\bullet(HOMO)/PTFE\ (LUMO),2}$ is 0.01375, and it is assigned to low $^{norm}I_{PE^{-}(HOMO)}$ (0.01375) compared with that of high $^{norm}I^{\bullet}_{PTFE\ (LUMO)}$ (0.10375). $C^{norm}TRfE_{PE^{-}\bullet(HOMO)/PTFE\ (LUMO),2}$ is defined as $^{norm}TRfE_{PE^{-}\bullet(HOMO)/PTFE\ (LUMO),2}$ with a charge sign. $C^{norm}TRfE_{PE^{-}(HOMO)/PTFE^{\bullet}(LUMO),2}$ is −0.01375. These terms are presented in Table 4 in the pathway line, Arabic numeral 2.

All the cases involving the soft contacting of $PE_{don,i}$ with $PTFE_{acc,i}$ are listed in Table 4 (pathway lines, Arabic numerals 1–16). Although the total number of pathways were 16, we emphasized that $^{Fe}PE_{don,i}$ could donate an *f-electron* to $^{Fe}PTFE_{acc,i}$ in the settings where $\Delta E_{FePEdon,i/FePTFEacc,i}$ > 0, i.e., $E_{FePEdon,i}$ > $E_{FePTFEacc,i}$. Accordingly, each $^{norm}TRfE_{FePEdon,i/FePTFEacc,i}$ was obtained in the settings where $E_{FePEdon,i}$ > $E_{FePTFEacc,i}$, i.e., those in which $^{norm}TRfE_{FePEdon,i/FePTFEacc,i}$ was assigned to low $^{norm}I_{ch.source,i}$ compared with high $^{norm}I_{ch.source,i}$. The feasible *f-electron* transfer pathways are presented in Table 4 (Pathways 2, 3, 4, 7, 8, 10, 11 and 12). $PE_{don,i}$, $PTFE_{acc,i}$, $E_{PEdon,i}$, $E_{PTFEacc,i}$, $\Delta E_{PEdon,i/PTFEacc,i}$, $^{Fe}PE_{don,i}$, $^{Fe}PTFE_{acc,i}$, $^{norm}TRfE_{FePEdon,i/FePTFEacc,i}$, and $C^{norm}TRfE_{FePEdon,i/FePTFEacc,i}$ are presented in Table 4 (Pathway numerals). Furthermore, $^{Total,norm}TRfE_{FePEdon,i/FePTFEacc,i}$ (0.39500) was obtained from the sum of $^{norm}TRfE_{FePEdon,i/FePTFEacc,i}$s. $C^{Total,norm}TRfE_{FePEdon,i/FePTFEacc,i}$ (−0.39500) was the $^{Total,norm}TRfE_{FePEdon,i/FePTFEacc,i}$ with charge sign.

Regarding these feasible *f-electron* transfer pathways, $C^{Total,norm}TRfE_{FePEdon,i/FePTFEacc,i}$ (−0.39500) is obtained via the *f-electron* transfer pathways of $^{Total}N_{FePEdon,i/FePTFEacc,i}$ (8) in the settings where $\Delta^{Total}E_{FePEdon,i/FePTFEacc,i}$ (2.08694 a.u.) = {$^{Total}E_{FePEdon,i}$ (−0.21254 a.u.) – $^{Total}E_{FePTFEacc,i}$ (−2.29948 a.u.)} > 0.

We emphasized that $C^{Total,norm}TRfE_{FePEdon,i/FePTFEacc,i}$ (−0.39500) indicates the amount of the normalized transferred *f-electron* from $^{Total,Fe}PE_{don,i}$ to $^{Total,Fe}PTFE_{acc,i}$ via the $^{Total}N_{FePEdon,i/FePTFEacc,i}$ (8) in the settings where $^{Total}E_{FePEdon,i}$ (−0.21254 a.u.) > $^{Total}E_{FePTFEacc,i}$ (−2.29948 a.u.).

Second, we considered *f-electron* transfer from $PTFE_{don,i}$ to $PE_{acc,i}$ in a vacuum.

For example, regarding the soft contacting of $PTFE^{-}$(HOMO) with $PE^{\bullet}$(LUMO), the transfer of an *f-electron* from $PTFE^{-}$(HOMO) as the donor to $PE^{\bullet}$(LUMO) as the acceptor can be achieved without additional extra-energy because $\Delta E_{PTFE^{-}\bullet(HOMO)/PE\ (LUMO),18}$ = $-E_{PTFE^{-}(HOMO)}$ (0.09858) - $E^{\bullet}_{PE\ (LUMO)}$ (−0.05110) = 0.14968 > 0.00000 a.u., and the density lobes at the C_2– and C_3-atoms of the $PTFE^{-}$(HOMO) (Fig. 2b) and $PE^{\bullet}$(LUMO) (Fig. 1f), respectively, are large. This feasible *f-electron* transfer pathway is reported in Table 5 as $PTFE^{-}$(HOMO) → $PE^{\bullet}$(LUMO) (Pathway 18). Regarding this feasible *f-electron* transfer pathway, $^{norm}TRfE_{PTFE^{-}\bullet(HOMO)/PE\ (LUMO),18}$ is defined as the concentration of normalized transferred *f-electron* from $PTFE^{-}$(HOMO) as the donor to $PE^{\bullet}$(LUMO) as the acceptor. $^{norm}TRfE_{PTFE^{-}\bullet(HOMO)/PE\ (LUMO),18}$ is 0.02125, and $^{norm}TRfE_{PTFE^{-}(HOMO)/PE^{\bullet}\ (LUMO),18}$ is assigned to low $^{norm}I_{PTFE^{-}(HOMO)}$ (0.02125) compared with high $^{norm}I^{\bullet}_{PE\ (LUMO)}$ (0.11125). $C^{norm}TRfE_{PTFE^{-}\bullet(HOMO)/PE\ (LUMO),18}$ is defined as $^{norm}TRfE_{PTFE^{-}\bullet(HOMO)/PE\ (LUMO),18}$ with a charge sign. $C^{norm}TRfE_{PTFE^{-}(HOMO)/PE\bullet(LUMO),18}$ is −0.02125. These two terms are listed in Table 5 (Pathway 18).

All the cases regarding the soft contacting of $PTFE_{don,i}$ with $PE_{acc,i}$ are reported in Table 5 (Pathways 17–32). Although the total number of Pathways were 16, we emphasized that $^{Fe}PTFE_{don,i}$ could donate an *f-electron* to $^{Fe}PE_{acc,i}$ in the settings where $\Delta E_{FePTFEdon,i/FePEacc,i}$ > 0, i.e., $E_{FePTFEdon,i}$ > $E_{FePEacc,i}$. Accordingly, each $^{norm}TRfE_{FePTFEdon,i/FePEacc,i}$ was obtained in the settings where $E_{FePTFEdon,i}$ > $E_{FePEacc,i}$, i.e., those in which $^{norm}TRfE_{FePTFEdon,i/FePEacc,i}$ was assigned to low $^{norm}I_{ch.source,i}$ compared with high $^{norm}I_{ch.source,i}$. The feasible *f-electron* transfer pathways are presented in Table 5 (Pathways 18, 19, 20, 24, 27, and 28). $PTFE_{don,i}$, $PE_{acc,i}$, $E_{PTFEdon,i}$, $E_{PEacc,i}$, $\Delta E_{PTFEdon,i/PEacc,i}$, $^{Fe}PTFE_{don,i}$, $^{Fe}PE_{acc,i}$, $^{norm}TRfE_{FePTFEdon,i/FePEacc,i}$, and $C^{norm}TRfE_{FePTFEdon,i/FePEacc,i}$ are presented in Table 5 (Pathway numerals). Further, $^{Total,norm}TRfE_{FePTFEdon,i/FePEacc,i}$ (0.187500) was obtained from the sum of $^{norm}TRfE_{FePTFEdon,i/FePEacc,i}$s. $C^{Total,norm}TRfE_{FePTFEdon,i/FePEacc,i}$ (−0.187500) was the $^{Total,norm}TRfE_{FePTFEdon,i/FePEacc,i}$ with charge sign.

Regarding these feasible *f-electron* transfer pathways, $C^{Total,norm}TRfE^{FePTFEdon,i/FePEacc,i}$ (−0.187500) is obtained via the *f-electron* transfer pathways of $^{Total}N_{FePTFEdon,i/FePEacc,i}$ (6) is in the settings where $\Delta^{Total}E_{FePTFEdon,i/FePEacc,i}$ (1.53927 a.u.) = {$^{Total}E_{FePTFEdon,i}$ (−0.13629 a.u.) – $^{Total}E_{FePEacc,i}$ (−1.67556 a.u.)} > 0.

We emphasized that the $C^{Total,norm}TRfE_{FePTFEdon,i/FePEacc,i}$ (−0.187500) indicated the amount of the normalized transferred-*f-electron* from $^{Total,Fe}PTFE_{don,i}$ to $^{Total,Fe}PE_{acc,i}$ via the $^{Total}N_{FePTFEdon,i/FePEacc,i}$ (6) in the settings where $^{Total}E_{FePTFEdon,i}$ (−0.13629 a.u.) > $^{Total}E_{FePEacc,i}$ (−1.67556 a.u.).

Next, after soft contacting, we speculated a normalized net surface charge of PE ($^{Net.norm}SC_{soft,Av.PE}$) and that of PTFE ($^{Net.norm}SC_{soft,Av.PTFE}$) based on the $C^{Total,norm}TRfE_{FePEdon,i/FePTFEacc,i}$ (−0.39500) and $C^{Total,norm}TRfE_{FePTFEdon,i/FePEacc,i}$ (−0.187500).

Regarding the soft contacting, the $\Delta C^{Net.norm}TRfE$ is given as $\Delta C^{Net.norm}TRfE$ (−0.20750) = $C^{Total,norm}TRfE_{FePEdon,i/FePTFEacc,i}$ (−0.39

Table 4
Soft contacting between $PE_{don,i}$ and $PTFE_{acci}$, $E_{PEdon,i,}$ $\Delta E_{PEdon,i/PTFEacc,i}$, $^{Fe}PE_{don,i}$, $^{Fe}PTFE_{acc,i,}$ $^{norm}TRfE_{FePEdon,i/FePTFEacc,i,}$ and $C^{norm}TRfE_{FePEdon,i/FePTFEacc,i}$.

Path. No.	Soft contacting between $PE_{don,i}$ and $PTFE_{acc,i}$	$E_{PEdon,i}$ [a.u.]	$E_{PTFEacc,i}$ [a.u.]	$\Delta E_{PEdon,i/PTFEacc,i}$ [a.u.]	Feasible f-electron transfer pathway from $^{Fe}PE_{don,i}$ to $^{Fe}PTFE_{acc,i}$	$^{norm}TRfE_{FePEdon,i/FePTFEacc,i}$	$C^{norm}TRfE_{FePEdon,i/FePTFEacc,i}$
1	PE^{-}(HOMO) / $PTFE^{-}$(LUMO)	0.11694	0.26369	−0.14675		0.00000	0.00000
2	PE^{-}(HOMO) / $PTFE^{\bullet}$(LUMO)	0.11694	−0.09374	**0.21068**	PE^{-}**(HOMO) → PTFE$^{\bullet}$(LUMO)**	**0.01375**	**−0.01375**
3	PE^{-}(HOMO) / $PTFE^{\bullet}$(HOMO)	0.11694	−0.24455	**0.36149**	PE^{-}**(HOMO) → PTFE$^{\bullet}$(HOMO)**	**0.01375**	**−0.01375**
4	PE^{-}(HOMO) / $PTFE^{+}$(LUMO)	0.11694	−0.45945	**0.57639**	PE^{-}**(HOMO) → PTFE^{+}(LUMO)**	**0.01375**	**−0.01375**
5	$PE^{\bullet}$(HOMO) / $PTFE^{-}$(LUMO)	−0.20503	0.26369	−0.46872		0.00000	0.00000
6	$PE^{\bullet}$(HOMO) / $PTFE^{\bullet}$(LUMO)	−0.20503	−0.09374	−0.11129		0.00000	0.00000
7	$PE^{\bullet}$(HOMO) / $PTFE^{\bullet}$(HOMO)	−0.20503	−0.24455	**0.03952**	**PE$^{\bullet}$(HOMO) → PTFE$^{\bullet}$(HOMO)**	**0.10375**	**−0.10375**
8	$PE^{\bullet}$(HOMO) / $PTFE^{+}$(LUMO)	−0.20503	−0.45945	**0.25442**	**PE$^{\bullet}$(HOMO) → PTFE^{+}(LUMO)**	**0.02125**	**−0.02125**
9	$PE^{\bullet}$(LUMO) / $PTFE^{-}$(LUMO)	−0.05110	0.26369	−0.31479		0.00000	0.00000
10	$PE^{\bullet}$(LUMO) / $PTFE^{\bullet}$(LUMO)	−0.05110	−0.09374	**0.04264**	**PE$^{\bullet}$(LUMO) → PTFE$^{\bullet}$(LUMO)**	**0.10375**	**−0.10375**
11	$PE^{\bullet}$(LUMO) / $PTFE^{\bullet}$(HOMO)	−0.05110	−0.24455	**0.19345**	**PE$^{\bullet}$(LUMO) → PTFE$^{\bullet}$(HOMO)**	**0.10375**	**−0.10375**
12	$PE^{\bullet}$(LUMO) / $PTFE^{+}$(LUMO)	−0.05110	−0.45945	**0.40835**	**PE$^{\bullet}$(LUMO) → PTFE^{+}(LUMO)**	**0.02125**	**−0.02125**
13	PE^{+}(HOMO) / $PTFE^{-}$(LUMO)	−0.57603	0.26369	−0.83972		0.00000	0.00000
14	PE^{+}(HOMO) / $PTFE^{\bullet}$(LUMO)	−0.57603	−0.09374	−0.48229		0.00000	0.00000
15	PE^{+}(HOMO) / $PTFE^{\bullet}$(HOMO)	−0.57603	−0.24455	−0.33148		0.00000	0.00000
16	PE^{+}(HOMO) / $PTFE^{+}$(LUMO)	−0.57603	−0.45945	−0.11658		0.00000	0.00000

Table 5
Soft contacting between $PTFE_{don,i}$ and $PE_{acc,i,}$ $E_{PTFEdon,i,}$ $E_{PEacc,i}$, $\Delta E_{PTFEdon,i/PEacc,i}$, $^{Fe}PTFE_{don,i}$, $^{Fe}PE_{acc,i}$, $^{norm}TRfE_{FePTFEdon,i/FePEacc,i}$, and $C^{norm}TRfE_{FePTFEdon,i/FePEacc,i}$.

Path. No.	Soft contacting between $PTFE_{don,i}$ and $PE_{acc,i}$	$E_{PTFEdon,i}$ [a.u.]	$E_{PEacc,i}$ [a.u.]	$\Delta E_{PTFEdon,i/PEacc,i}$ [a.u.]	Feasible f-electron transfer pathway from $^{Fe}PTFE_{don,i}$ to $^{Fe}PE_{acc,i}$	$^{norm}TRfE_{FePTFEdon,i/FePEacc,i}$	$C^{norm}TRfE_{FePTFEdon,i/FePEacc,i}$
17	$PTFE^{-}$(HOMO) / PE^{-}(LUMO)	0.09858	0.22878	−0.13020		0.00000	0.00000
18	$PTFE^{-}$(HOMO) / $PE^{\bullet}$(LUMO)	0.09858	−0.05110	**0.14968**	**PTFE^{-}(HOMO) → PE$^{\bullet}$(LUMO)**	**0.02125**	**−0.02125**
19	$PTFE^{-}$(HOMO) / $PE^{\bullet}$(HOMO)	0.09858	−0.20503	**0.30361**	**PTFE^{-}(HOMO) → PE$^{\bullet}$(HOMO)**	**0.02125**	**−0.02125**
20	$PTFE^{-}$(HOMO) / PE^{+}(LUMO)	0.09858	−0.40480	**0.50338**	**PTFE^{-}(HOMO) → PE^{+}(LUMO)**	**0.01375**	**−0.01375**
21	$PTFE^{\bullet}$(HOMO) / PE^{-}(LUMO)	−0.24455	0.22878	−0.47333		0.00000	0.00000
22	$PTFE^{\bullet}$(HOMO) / $PE^{\bullet}$(LUMO)	−0.24455	−0.05110	−0.19345		0.00000	0.00000
23	$PTFE^{\bullet}$(HOMO) / $PE^{\bullet}$(HOMO)	−0.24455	−0.20503	−0.03952		0.0000	0.0000
24	$PTFE^{\bullet}$(HOMO) / PE^{+}(LUMO)	−0.24455	−0.40480	**0.16025**	**PTFE$^{\bullet}$**(HOMO) → **PE^{+}(LUMO)**	**0.01375**	**−0.01375**
25	$PTFE^{\bullet}$(LUMO) / PE^{-}(LUMO)	−0.09374	0.22878	−0.32252		0.00000	0.00000
26	$PTFE^{\bullet}$(LUMO) / $PE^{\bullet}$(LUMO)	−0.09374	−0.05110	−0.04264		0.00000	0.00000
27	$PTFE^{\bullet}$(LUMO) / $PE^{\bullet}$(HOMO)	−0.09374	−0.20503	**0.11129**	**PTFE$^{\bullet}$(LUMO) → PE$^{\bullet}$(HOMO)**	**0.10375**	**−0.10375**
28	$PTFE^{\bullet}$(LUMO) / PE^{+}(LUMO)	−0.09374	−0.40480	**0.31106**	**PTFE$^{\bullet}$(LUMO) → PE^{+}(LUMO)**	**0.01375**	**−0.01375**
29	$PTFE^{+}$(HOMO) / PE^{-}(LUMO)	−0.61472	0.22878	−0.84350		0.00000	0.00000
30	$PTFE^{+}$(HOMO) / $PE^{\bullet}$(LUMO)	−0.61472	−0.05110	−0.56362		0.00000	0.00000
31	$PTFE^{+}$(HOMO) / $PE^{\bullet}$(HOMO)	−0.61472	−0.20503	−0.40969		0.00000	0.00000
32	$PTFE^{+}$(HOMO) / PE^{+}(LUMO)	−0.61472	−0.40480	−0.20992		0.00000	0.00000

500) – $C^{Total,norm}TRfE_{FePTFEdon,i/FePEacc,i}$ (−0.18750). Accordingly, $\Delta C^{Net.norm}TRfE$ (−0.20750) is obtained via feasible *f-electron* transfer pathways in the settings where

$$\begin{aligned}&\Delta^{Total}E\ (0.54767\ \text{a.u.})\\&=\Delta^{Total}E_{FePEdon,i/FePTFEacc,i}\ (2.08694\ \text{a.u.})-\Delta^{Total}E_{FePTFEdon,i/FePEacc,i}\ (1.53927\ \text{a.u.})\\&=\left\{{}^{Total}E_{FePEdon,i}(-0.21254\text{a.u.})+{}^{Total}E_{FePEacc,i}(-1.67556\text{a.u.})\right\}\\&\quad-\left\{{}^{Total}E_{FePTFEdon,i}(-0.13629\text{a.u.})+{}^{Total}E_{FePTFEacc,i}(-2.29948\text{a.u.})\right\}\\&={}^{Total}E_{whole,FePEdon,i}(-1.88810\text{a.u.})-{}^{Total}E_{whole,FePTFEacc,i}(-2.43577\text{a.u.})>0\end{aligned}\quad(5)$$

By introducing ${}^{Total}N_{whole,FePEdon,i}$ (14), and ${}^{Total}N_{whole,FePTFEacc,i}$ (14) into Eq. (5), the next equation would be obtained, as follows:

$$\begin{aligned}&=\{{}^{Total}E_{whole,FePEdon,i}\ (-1.88810\ \text{a.u.})/\ {}^{Total}N_{whole,FePEdon,i}\ (14)\}\times{}^{Total}N_{whole,FePEdon,i}\ (14)-\{{}^{Total}E_{whole,FePTFEacc,i}\ (-2.43577\ \text{a.u.})/\ {}^{Total}N_{whole,FePTFEacc,i}\ (14)\}\times{}^{Total}N_{whole,FePTFEacc,i}\ (14).\\&=E_{Av.whole,FePEdon,i}\ (-0.13486\ \text{a.u.})\times{}^{Total}N_{whole,FePEdon,i}\ (14)\\&\quad-E_{Av.whole,FePTFEacc,i}(-0.17398\ \text{a.u.})\times{}^{Total}N_{whole,FePTFEacc,i}(14)>0\end{aligned}\quad(6)$$

Therefore, $\Delta C^{Net.norm}TRfE$ (−0.20750) is obtained from the settings, where $E_{Av.whole,FePEdon,i}$ (−0.13486 a.u.) > $E_{Av.whole,FePTFEacc,i}$ (−0.17398 a.u.).

We concluded that the PE surface comprising ${}^{whole,Fe}PE_{don,i}$ donated the *f-electrons* of $\Delta C^{Net.norm}TRfE$(−0.20750) to ${}^{whole,Fe}PTFE^{acc,i}$ via the feasible *f-electron* transfer pathways in the settings, where $E_{Av.whole,FePEdon,i}$ (−0.13486 a.u.) > $E_{Av.whole,FePTFEacc,i}$ (−0.17398 a.u.). Consequently, the PE surface resulted in the *positive net surface charge of PE* (*PE(+)*) with ${}^{Net.norm}SC_{soft,Av.PE}$(+0.20750). Although the PTFE surface comprising ${}^{whole,Fe}PTFE^{acc,i}$ accepts *f-electrons* of $\Delta C^{Net.norm}TRfE$(−0.20750), and results in *negative net surface charge of PTFE* (*PTFE(−)*) with ${}^{Net.norm}SC_{soft,Av.PTFE}$(−0.20750).

Here, we proposed the following charging mechanism of CE between PE and PTFE in a vacuum without the decay of the charge sources (illustrated in Fig. 3). Before "Hard Contacting," the PE and PTFE surfaces did not exhibit any electric charge. Stage 1.H.C.: The "Hard Contacting," between PE and PTFE produces $PE_{ch.source,i}$−{PE^-(HOMO), PE^+(HOMO), PE^-(LUMO), PE^+(LUMO), $PE^\bullet$(HOMO), $PE^\bullet$(LUMO)} on the PE surface and $PTFE_{ch.source,i}${$PTFE^-$(HOMO), $PTFE^+$(HOMO), $PTFE^-$(LUMO), $PTFE^+$(LUMO), $PTFE^\bullet$(HOMO), $PTFE^\bullet$(LUMO)} on the PTFE surface. PE (+, −, •) and PTFE(+, −, •) refer to $PE_{ch.source,i}$ and $PTFE_{ch.source,i}$, respectively. Although each surface-charge profile of PE or PTFE is exhibited as a non-uniform charge pattern arising from $PE_{ch.souce,i}$ or $PTFE_{ch.souece,i}$, respectively, ${}^{Total,norm}SC_{hard,PEch.source,i}$ and ${}^{Total,norm}SC_{hard,PTFEch.source,i}$ are 0.00000, i.e., each surface charge is neutral. Stage 2.S.C.: "Soft Contacting," which refers to contacting without covalent bond scissions, between $PE_{ch.source,i}$ and $PTFE_{ch.souece,i}$ can induce *f-electron* transfer between $PE_{ch.source,i}$ and $PTFE_{ch.souece,i}$. Regarding soft contacting, all the contact combinations between $PE_{ch.source,i}$ and $PTFE_{ch.source,i}$ were considered in 32 combinations. One category comprises 16 combinations of $PE_{don,i}$ and $PTFE_{acc,i}$, i.e., 16 pathways that might account for *f-electron* transfer from $PE_{don,i}$ to $PTFE_{acc,i}$. We assumed that the transfer of *f-electron* from $PE_{don,i}$ to $PTFE_{acc,i}$ will be executed if $E_{PEdon,i}$ is higher than $E_{PTFEacc,i}$, where the activation energy of *f-electron* transfer reaction is zero. Although the total number of pathways are 16, ${}^{Fe}PE_{don,i}$ can donate *f-electron* to ${}^{Fe}PTFE_{acc,i}$ because $E_{FePEdon,i}$ > $E_{FePTFEacc,i}$. $C^{Total,norm}TRfE^{FePEdon,i/FePTFEacc,i}$ (−0.39500) indicates the amount of the normalized transferred *f-electron* from ${}^{Total,Fe}PE_{don,i}$ to ${}^{Total,Fe}PTFE_{acc,i}$ via the ${}^{Total}N_{FePEdon,i/FePTFEacc,i}$ (8) in the settings where ${}^{Total}E_{FePEdon,i}$ (−0.21254 a.u.) > ${}^{Total}E_{FePTFEacc,i}$ (−2.29948 a.u.). Another category comprises 16 combinations of $PTFE_{don,i}$ and $PE_{acc,i}$. $C^{Total,norm}TRfE^{FePTFEdon,i/FePEacc,i}$ (−0.187500) indicated the amount of the normalized transferred-*f-electron* from ${}^{Total,Fe}PTFE_{don,i}$ to ${}^{Total,Fe}PE_{acc,i}$ via the ${}^{Total}N_{FePTFEdon,i/FePEacc,i}$ (6) in the settings where ${}^{Total}E_{FePTFEdon,i}$ (−0.13629 a.u.) > ${}^{Total}E_{FePEacc,i}$ (−1.67556 a.u.). Thus, $\Delta C^{Net.norm}TRfE$(−0.20750) = {$C^{Total,norm}TRfE_{FePEdon,i/FePTFEacc,i}$ (−0.39500) – $C^{Total,norm}TRfE_{FeFTFEdon,i/FePEacc,i}$ (−0.18750)} is obtained from the *f-electron* transfer from ${}^{whole,Fe}PE_{don,i}$ to ${}^{whole,Fe}PTFE_{acc,i}$ in the setting, where $E_{Av.whole,FePEdon,i}$ (−0.13486 a.u.) > $E_{Av.whole,FePTFEacc,i}$ (−0.17398 a.u.). Consequently, the PE surface comprising ${}^{whole,Fe}PE^{don,i}$ donated the *f-electrons* of $\Delta C^{Net.norm}TRfE$ (−0.20750) to obtain the *positive net surface charge of PE* (*PE(+)*) with ${}^{Net.norm}SC_{soft,Av.whole,FePEdon,i}$ (+0.20750). However, the PTFE surface comprising ${}^{whole,Fe}PTFE^{acc,i}$ accepts *f-electrons* of $\Delta C^{Net.norm}TRfE$(−0.20750) to obtain the *negative net surface charge of PTFE* (*PTFE(-)*) with ${}^{Net.norm}SC^{soft,Av.PTFE}$(−0.20750). The non-uniform surface charge patterns of PE(+) and PTFE(−) were altered compared with that before soft contacting. Stage 3.Sep: After soft contacting, they might be separated infinitely on a molecular scale. They might not be encountered each other. We consider that this process for Stage 1 to 3 is one set of contacting process. For conventional CE, many sets of contacting might be executed on the surface at a molecular scale.

Next, after soft contact, we estimated the net amounts of the surface charges of PE and PTFE per square meter.

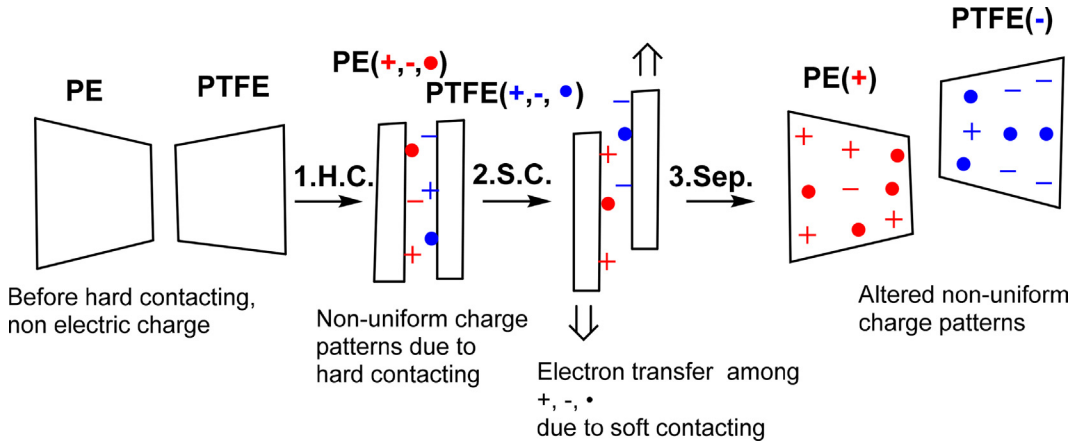

Fig. 3. Illustration of CE between PE and PTFE in a vacuum.

Table 6
Soft contacting between $PE_{don,i}$ and $PVC_{acc,i}$, $E_{PEdon,i}$, $E_{PVCacc,i}$, $\Delta E_{PEdon,i/PVCacc,i}$, $^{Fe}PE_{don,i}$, $^{Fe}PVC_{acc,i}$, $^{norm}TRfE_{PEdon,i/PVCacc,i}$, and $C^{norm}TRfE_{PEdon,i/PVCacc,i}$.

Path. No.	Soft contacting between $PE_{don,i}$ and $PVC_{acc,i}$	$E_{PEdon,i}$ [a.u.]	$E_{PVCacc,i}$ [a.u.]	$\Delta E_{PEdon,i/PVCacc,i}$ [a.u.]	Feasible f-electron transfer pathway from $^{Fe}PE_{don,i}$ to $^{Fe}PVC_{acc,i}$	$^{norm}TRfE_{PEdon,i/PVCacc,i}$	$C^{norm}TRfE_{PEdon,i/PVCacc,i}$
33	PE^{-}(HOMO) / $PVC1^{-}$(LUMO)	0.11694	0.19426	−0.07732		0.00000	0.00000
34	PE^{-}(HOMO) / $PVC2^{-}$(LUMO)	0.11694	0.21606	−0.09912		0.000000	0.000000
35	PE^{-}(HOMO) / $PVC1^{\bullet}$(LUMO)	0.11694	−0.08577	**0.20271**	PE^{-}**(HOMO) → PVC1$^{\bullet}$(LUMO)**	**0.006875**	**−0.006875**
36	PE^{-}(HOMO) / $PVC1^{\bullet}$(HOMO)	0.11694	−0.22376	**0.34070**	PE^{-}**(HOMO) → PVC1$^{\bullet}$(HOMO)**	**0.006875**	**−0.006875**
37	PE^{-}(HOMO) / $PVC2^{\bullet}$(LUMO)	0.11694	−0.07229	**0.18923**	PE^{-}**(HOMO) → PVC2$^{\bullet}$(LUMO)**	**0.006875**	**−0.006875**
38	PE^{-}(HOMO) / $PVC2^{\bullet}$(HOMO)	0.11694	−0.22663	**0.34357**	PE^{-}**(HOMO) → PVC2$^{\bullet}$(HOMO)**	**0.006875**	**−0.006875**
39	PE^{-}(HOMO) / $PVC1^{+}$(LUMO)	0.11694	−0.39067	**0.50761**	PE^{-}**(HOMO) → PVC1^{+}(LUMO)**	**0.006875**	**−0.006875**
40	PE^{-}(HOMO)) /$PVC2^{+}$(LUMO)	0.11694	−0.41251	**0.52945**	PE^{-}**(HOMO) → PVC2^{+}(LUMO)**	**0.006875**	**−0.006875**
41	$PE^{\cdot}$(HOMO) / $PVC1^{-}$(LUMO)	−0.20503	0.19426	−0.39929		0.000000	0.000000
42	$PE^{\bullet}$(HOMO) / $PVC2^{-}$(LUMO)	−0.20503	0.21606	−0.42109		0.000000	0.000000
43	$PE^{\bullet}$(HOMO) / $PVC1^{\bullet}$(LUMO)	−0.20503	−0.08577	−0.11926		0.000000	0.000000
44	$PE^{\bullet}$(HOMO) / $PVC1^{\bullet}$(HOMO)	−0.20503	−0.22376	**0.01873**	**PE$^{\bullet}$(HOMO) → PVC1$^{\bullet}$(HOMO)**	**0.031250**	**−0.031250**
45	$PE^{\bullet}$(HOMO) / $PVC2^{\bullet}$(LUMO)	−0.20503	−0.07229	−0.13274		0.000000	0.000000
46	$PE^{\bullet}$(HOMO) / $PVC2^{\bullet}$(HOMO)	−0.20503	−0.22663	**0.02160**	**PE$^{\bullet}$(HOMO) → PVC2$^{\bullet}$(HOMO)**	**0.031250**	**−0.031250**
47	$PE^{\bullet}$(HOMO) / $PVC1^{+}$(LUMO)	−0.20503	−0.39067	**0.18564**	**PE$^{\bullet}$(HOMO) → PVC1^{+}(LUMO)**	**0.031250**	**−0.031250**
48	$PE^{\bullet}$(HOMO) / $PVC2^{+}$(LUMO)	−0.20503	−0.41251	**0.20748**	**PE$^{\bullet}$(HOMO) → PVC2^{+}(LUMO)**	**0.031250**	**−0.031250**
49	$PE^{\bullet}$(LUMO) / $PVC1^{-}$(LUMO)	−0.05110	0.19426	−0.24536		0.000000	0.000000
50	$PE^{\bullet}$(LUMO) / $PVC2^{-}$(LUMO)	−0.05110	0.21606	−0.26716		0.000000	0.000000
51	$PE^{\bullet}$(LUMO) / $PVC1^{\bullet}$(LUMO)	−0.05110	−0.08577	**0.03467**	**PE$^{\bullet}$(LUMO) → PVC1$^{\bullet}$(LUMO)**	**0.031250**	**−0.031250**
52	$PE^{\bullet}$(LUMO) / $PVC1^{\bullet}$(HOMO)	−0.05110	−0.22376	**0.17266**	**PE$^{\bullet}$(LUMO) → PVC1$^{\bullet}$(HOMO)**	**0.031250**	**−0.031250**
53	$PE^{\bullet}$(LUMO) / $PVC2^{\bullet}$(LUMO)	−0.05110	−0.07229	**0.02119**	**PE$^{\bullet}$(LUMO) → PVC2$^{\bullet}$(LUMO)**	**0.031250**	**−0.031250**
54	$PE^{\bullet}$(LUMO) / $PVC2^{\bullet}$(HOMO)	−0.05110	−0.22663	**0.17553**	**PE$^{\bullet}$(LUMO) → PVC2$^{\bullet}$(HOMO)**	**0.031250**	**−0.031250**
55	$PE^{\bullet}$(LUMO) / $PVC1^{+}$(LUMO)	−0.05110	−0.39067	**0.33957**	**PE$^{\bullet}$(LUMO) → PVC1^{+}(LUMO)**	**0.031250**	**−0.031250**
56	$PE^{\bullet}$(LUMO) / $PVC2^{+}$(LUMO)	−0.05110	−0.41251	**0.36141**	**PE$^{\bullet}$(LUMO) → PVC2^{+}(LUMO)**	**0.031250**	**−0.031250**
57	PE^{+}(HOMO) / $PVC1^{-}$(LUMO)	−0.57603	0.19426	−0.77029		0.000000	0.000000
58	PE^{+}(HOMO) / $PVC2^{-}$(LUMO)	−0.57603	0.21606	−0.79209		0.000000	0.000000
59	PE^{+}(HOMO) / $PVC1^{\bullet}$(LUMO)	−0.57603	−0.08577	−0.49026		0.000000	0.000000
60	PE^{+}(HOMO) / $PVC1^{\bullet}$(HOMO)	−0.57603	−0.22376	−0.35227		0.000000	0.000000
61	PE^{+}(HOMO) / $PVC2^{\bullet}$(LUMO)	−0.57603	−0.07229	−0.50374		0.000000	0.000000
62	PE^{+}(HOMO) / $PVC2^{\bullet}$(HOMO)	−0.57603	−0.22663	−0.34940		0.000000	0.000000
63	PE^{+}(HOMO) / $PVC1^{+}$(LUMO)	−0.57603	−0.39067	−0.18536		0.000000	0.000000
64	PE^{+}(HOMO) / $PVC2^{+}$(LUMO)	−0.57603	−0.41251	−0.16352		0.000000	0.000000

In previous section, we obtained $^{Total}I_{f\text{-}e,PTFE}$(3.9013 × 10^{16} [f-electron/m^2]), and we assumed that $^{Total}I_{f\text{-}e,PE}$ = $^{Total}I_{f\text{-}e,PTFE}$. Thus, $\Delta C^{Net.norm}$TRfE(−0.20750) was estimated as −8.09524 × 10^{15} [f-electron/m^2]. Assuming that one *f-electron* was equal to the elementary charge of one electron (1.602177 × 10^{-19} [C]). Thus, $\Delta C^{Net.norm}$TRfE (−8.09524 × 10^{15} [f-electron/m^2]) was estimated as −1.2970 × 10^{-3} [C/m^2]. Namely, PE donated −1.2970 × 10^{-3} [C/m^2] to PTFE, and results in PE(+) with a positive charge (+1.2970 × 10^{-3} [C/m^2]). However, PTFE accepted −1.2970 × 10^{-3} [C/m^2] to obtain PTFE(−) with a negative charge (−1.2970 × 10^{-3} [C/m^2]).

Contrarily, Soh et al. reported that the charge value of PTFE induced by CE was PTFE(−) = −6.7 [μC/m^2]; there in, the materials were contacted 60 times [27]. Conversely, our result for PTFE (−1.2970 × 10^{-3} [C/m^2]) was over two orders of magnitude higher than that by Soh et al. (−6.7 [μC/m^2]). This large value might be due to the large concentration of $^{Total}I_{f\text{-}e,PTFE}$(3.9013 × 10^{16} [f-electron/m^2], which was produced during vibratory ball-milling in a vacuum for 21 h at 77 K with 5 Hz. Additionally, in our experiment, charge leaking, the decay of the charge sources, as well as the effects of water and temperature, were abrogated.

3.2.2. CE of PE and PVC in vacuum

We discussed CE of PE and PVC based on the *f-electron* transfer between $PE_{ch.source,i}$ and $PVC_{ch.source,i}$ in a vacuum.

First, we considered the hard contact between PE and PVC in a vacuum. $PE_{ch.source,i}$ and $PVC_{ch.source,i}$ were produced and anchored to the PE and PVC surfaces via hard contacting. Consequently, the PE and PVC surfaces exhibited charge-mosaic patterns comprising nano-scale regional charges from $PE_{ch.source,i}$ and $PVC_{ch.source,i}$. Although both surfaces exhibited charge-mosaic patterns, $^{Total,norm}SC_{hard,PEch.source,i}$ and $^{Total,norm}SC_{hard,PVCch.source,i}$ were 0.00000 (neutral).

Second, we considered the soft contact between $PE_{ch.source,i}$ and $PVC_{ch.source,i}$ in a vacuum. A total of 64 combinations were considered for all the possible contact between $PE_{ch.source,i}$ and $PVC_{ch.source,i}$, and they were divided into two categories. One category composed 32 combinations of $PE_{don,i}$ and $PVC_{acc,i}$, i.e., 32 pathways might account for *f-electron* transfer from $PE_{don,i}$ to $PVC_{acc,i}$. Another category comprised 32 combinations of $PVC_{don,i}$ and $PE_{acc,i}$, i.e., 32 pathways might account for *f-electron* transfer from $PVC_{don,i}$ to $PE_{acc,i}$. Regarding the soft contacting, we assumed that the total *f-electrons* of $PVC_{ch.source,i}$ ($^{Total}I_{f\text{-}e,PVC}$) were identical to the $^{Total}I_{f\text{-}e,PE}$, indicating that $^{norm}I_{PEch.source,i}$ and $^{norm}I_{PVCch.source,i}$ were normalized to the products by eight-time scissions.

First, we considered *f-electron* transfer from $PE_{don,i}$ to $PVC_{acc,i}$ in a vacuum.

All the cases involving the soft contact of $PE_{don,i}$ with $PVC_{acc,i}$ are presented in Table 6 in (Pathways 33 –64). Although the total number of pathways were 32, we emphasized that $^{Fe}PE_{don,i}$ could donate *f-electron* to $^{Fe}PVC_{acc,i}$ in settings where $\Delta E_{FePEdon,i/FePVCacc,i}$ > 0, i.e., $E_{FePEdon,i}$ > $E_{FePVCacc,i}$. Accordingly, each $^{norm}TRfE_{FePEdon,i/FePVCacc,i}$ was obtained in settings where $E_{FePEdon,i}$ > $E_{FePVCacc,i}$, i.e., those in which $^{norm}TRfE_{FePEdon,i/FePVCacc,i}$ was assigned to low $^{norm}I_{ch.source,i}$ compared with high $^{norm}I_{ch.source,i}$. The feasible *f-electron* transfer pathways are presented in Table 6 (Pathways 35, 36, 37, 38, 39, 40, 44, 46, 47, 48, 51, 52, 53, 54, 55, and 56). $PE_{don,i}$, $PVC_{acc,i}$, $E_{PEdon,i}$, $E_{PVCacc,i}$, $\Delta E_{PEdon,i/PVCacc,i}$, $^{Fe}PE_{don,i}$, $^{Fe}PVC_{acc,i}$, $^{norm}TRfE_{FePEdon,i/FePVCacc,i}$, and $C^{norm}TRfE_{FePEdon,i/FePVCacc,i}$ are presented in Table 6 (Pathways numerals). Further, $^{Total,norm}TRfE_{FePEdon,i/FePVCacc,i}$ (0.353750) was obtained from the sum of $^{norm}TRfE_{FePEdon,i/FePVCacc,i}$s. $C^{Total,norm}TRfE_{FePEdon,i/FePVCacc,i}$ (−0.353750) was the $^{Total,norm}TRfE_{FePEdon,i/FePVCacc,i}$ with charge sign.

Regarding these feasible *f-electron* transfer pathways, $C^{Total,norm}TRfE^{FePEdon,i/FePVCacc,i}$ (−0.353750) was obtained via the *f-electron* transfer pathways of $^{Total}N_{FePEdon,i/FePVCacc,i}$ (16) in the settings, where $\Delta^{Total}E_{FePEdon,i/FePVCacc,i}$ (3.65175 a.u.) = {$^{Total}E_{FePEdon,i}$ (−0.42508 a.u.) − $^{Total}E_{FePVCacc,i}$ (−4.07683 a.u.)} > 0.

We emphasized that $C^{Total,norm}TRfE_{FePEdon,i/FePVCacc,i}$ (−0.35375) indicated the amount of the normalized transferred-*f-electron* from $^{Total,Fe}PE_{don,i}$ to $^{Total,Fe}PVC_{acc,i}$ via the $^{Total}N_{FePEdon,i/FePVCacc,i}$ (16) in the settings where $^{Total}E_{FePEdon,i}$ (−0.42508 a.u.) > $^{Total}E_{FePVCacc,i}$ (−4.07683 a.u.).

Second, we considered *f-electron* transfer from $PVC_{don,i}$ to $PE_{acc,i}$ in a vacuum.

All the cases regarding the soft contacting of $PVC_{don,i}$ with $PE_{acc,i}$ are reported in Table 7 (Pathways 65 –96). Although the total number of Pathways are 32, we emphasized that $^{Fe}PVC_{don,i}$ could donate an *f-electron* to a $^{Fe}PE_{acc,i}$ in the settings where $\Delta E_{FePVCdon,i/FePEacc,i}$ > 0, i.e., $E_{FePVCdon,i}$ > $E_{FePEacc,i}$. Accordingly, each $^{norm}TRfE_{FePVCdon,i/FePEacc,i}$ is obtained in the settings where $E_{FePVCdon,i}$ > $E_{FePEacc,i}$, where $^{norm}TRfE_{FePVCdon,i/FePEacc,i}$ was assigned to low $^{norm}I_{ch.source,i}$ as compared with high $^{norm}I_{ch.source,i}$. The feasible *f-electron* transfer pathways are presented in Table 7 (Pathways 66, 67, 68, 70, 71, 72, 76, 79, 80, 84, 87, and 88). $PVC_{don,i}$, $PE_{acc,i}$, $E_{PVCdon,i}$, $E_{PEacc,i}$, $\Delta E_{PVCdon,i/PEacc,i}$, $^{Fe}PVC_{don,i}$, $^{Fe}PE_{acc,i}$, $^{norm}TRfE_{FePVCdon,i/FePEacc,i}$, and the $C^{norm}TRfE_{FePVCdon,i/FePEacc,i}$ are presented in Table 7 (Pathways numerals). Further, $^{Total,norm}TRfE_{FePVCdon,i/FePEacc,i}$ (0.228750) was obtained from the sum of $^{norm}TRfE_{FePVCdon,i/FePEacc,i}$s. $C^{Total,norm}TRfE_{FePVCdon,i/FePEacc,i}$ (−0.228750) was the $^{Total,norm}TRfE_{FePVCdon,i/FePEacc,i}$ with charge sign.

Regarding these feasible *f-electron* transfer pathways, $C^{Total,norm}TRfE^{FePVCdon,i/FePEacc,i}$ (−0.228750) is obtained via the *f-electron* transfer pathways of $^{Total}N_{FePVCdon,i/FePEacc,i}$ (12) in the settings where $\Delta^{Total}E_{FePVCdon,i/FePEacc,i}$ (3.06503 a.u.) = {$^{Total}E_{FePVCdon,i}$ (−0.28609 a.u.) − $^{Total}E_{FePEacc,i}$ (−3.35112 a.u.)} > 0.

We emphasized that the $C^{Total,norm}TRfE_{FePVCdon,i/FePEacc,i}$ (−0.228750) indicated the amount of the normalized transferred-*f-electron* from $^{Total,Fe}PVC_{don,i}$ to $^{Total,Fe}PE_{acc,i}$ via the $^{Total}N_{FePVCdon,i/FePEacc,i}$ (12) in the settings where $^{Total}E_{FePVCdon,i}$ (−0.28609 a.u.) > $^{Total}E_{FePEacc,i}$ (−3.35112 a.u.).

Next, after soft contacting, we speculated $^{Net.norm}SC_{soft,Av.PE}$ and a normalized net surface charge of PVC ($^{Net.norm}SC_{soft,Av.PVC}$) based on $C^{Total,norm}TRfE_{FePEdon,i/FePVCacc,i}$ (−0.353750) and $C^{Total,norm}TRfE^{FePVCdon,i/FePEacc,i}$ (−0.228750)

Regarding the soft contacting, $\Delta C^{Net.norm}$TRfE is given: $\Delta C^{norm}TRfE$ (−0.12500) = $C^{Total,norm}TRfE_{FePEdon,i/FePVCacc,i}$ (−0.353750) - $C^{Total,norm}TRfE_{FePVCdon,i/FePEacc,i}$ (−0.228750). Accordingly, $\Delta C^{Net.norm}$TRfE(−0.12500) is obtained via feasible *f-electron* transfer pathways in the settings where

$$\begin{aligned}&\Delta^{Total}E(0.58672\ \text{a.u.})\\&= \Delta^{Total}E_{FePEdon,i/FePVCacc,i}\ (3.65175\ \text{a.u.}) - \Delta^{Total}E_{FePVCdon,i/FePEacc,i}\ (3.06503\ \text{a.u.}).\\&= {}^{Total}E_{whole,FePEdon,i}(-3.77620\ a.u.) - {}^{Total}E_{whole,FePVCacc,i}(-4.36292\ a.u.)\\&> 0.\end{aligned} \tag{7}$$

By introducing $^{Total}N_{whole,FePEdon,i}$ (28), and $^{Total}N_{whole,FePVCacc,i}$ (28) into Eq. (7), the next equation would be obtained, as follows:

$$\begin{aligned}&= \{{}^{Total}E_{whole,FePEdon,i}\ (-3.77620\ \text{a.u.})/{}^{Total}N_{whole,FePEdon,i}\ (28)\} \times {}^{Total}N_{whole,FePEdon,i}\ (28) - \{{}^{Total}E_{whole,FePVCacc,i}\ (-4.36292\ \text{a.u.})/{}^{Total}N_{whole,FePVCacc,i}\ (28)\} \times {}^{Total}N_{whole,FePVCacc,i}\ (28).\\&= E_{Av.,FePEdon,i}(-0.13486 a.u.) \times {}^{Total}N_{whole,FePEdon,i}(28)\\&\quad - E_{Av.,FePVCacc,i}(-0.15582 a.u.) \times {}^{Total}N_{whole,FePVCacc,i}(28)\\&\quad > 0\end{aligned} \tag{8}$$

Table 7
Soft contacting between $PVC_{don,i}$ and $PE_{acc,i}$, $E_{PVCdon,i}$, $E_{PEacc,i}$, $\Delta E_{PVCdon,i/PEacc,i}$, $^{Fe}PVC_{don,i}$, $^{Fe}PE_{acc,i}$, $^{norm}TRfE_{PVCdon,i/PEacc,i}$, and $C^{norm}TRfE_{PVCdon,i/PEacc,i}$.

Path. No.	Soft contacting between $PVC_{don,i}$ and $PE_{acc,i}$	$E_{PVCdon,i}$ [a.u.]	$E_{PEacc,i}$ [a.u.]	$\Delta E_{PVCdon,i/PEacc,i}$ [a.u.]	Feasible f-electron transfer pathway from $^{Fe}PVC_{don,i}$ to $^{Fe}PE_{acc,i}$	$^{norm}TRfE_{PVCdon,i/PEacc,i}$	$C^{norm}TRfE_{PVCdon,i/PEacc,i}$
65	$PVC1^{-}$(HOMO) / PE^{-}(LUMO)	0.06700	0.22878	−0.16178		0.000000	0.000000
66	$PVC1^{-}$(HOMO) / $PE^{\bullet}$(LUMO)	0.06700	−0.05110	**0.11810**	**$PVC1^{-}$(HOMO) → $PE^{\bullet}$(LUMO)**	**0.031250**	**−0.031250**
67	$PVC1^{-}$(HOMO) / $PE^{\bullet}$(HOMO)	0.06700	−0.20503	**0.27203**	**$PVC1^{-}$(HOMO) → $PE^{\bullet}$(HOMO)**	**0.031250**	**−0.031250**
68	$PVC1^{-}$(HOMO) / PE^{+}(LUMO)	0.06700	−0.40480	**0.47180**	**$PVC1^{-}$(HOMO) → PE^{+}(LUMO)**	**0.006875**	**−0.006875**
69	$PVC2^{-}$(HOMO) / PE^{-}(LUMO)	0.09314	0.22878	−0.13564		0.000000	0.000000
70	$PVC2^{-}$(HOMO) / $PE^{\bullet}$(LUMO)	0.09314	−0.05110	**0.14424**	**$PVC2^{-}$(HOMO) → $PE^{\bullet}$(LUMO)**	**0.031250**	**−0.031250**
71	$PVC2^{-}$(HOMO) / $PE^{\bullet}$(HOMO)	0.09314	−0.20503	**0.29817**	**$PVC2^{-}$(HOMO) → $PE^{\bullet}$(HOMO)**	**0.031250**	**−0.031250**
72	$PVC2^{-}$(HOMO) / PE^{+}(LUMO)	0.09314	−0.40480	**0.49794**	**$PVC2^{-}$(HOMO) → PE^{+}(LUMO)**	**0.006875**	**−0.006875**
73	$PVC1^{\bullet}$(HOMO) / PE^{-}(LUMO)	−0.22376	0.22878	−0.45254		0.000000	0.000000
74	$PVC1^{\bullet}$(HOMO) / $PE^{\bullet}$(LUMO)	−0.22376	−0.05110	−0.17266		0.000000	0.000000
75	$PVC1^{\bullet}$(HOMO) / $PE^{\bullet}$(HOMO)	−0.22376	−0.20503	−0.01873		0.000000	0.000000
76	$PVC1^{\bullet}$(HOMO) / PE^{+}(LUMO)	−0.22376	−0.40480	**0.18104**	**$PVC1^{\bullet}$(HOMO) → PE^{+}(LUMO)**	**0.006875**	**−0.006875**
77	$PVC1^{\bullet}$(LUMO) / PE^{-}(LUMO)	−0.08577	0.22878	−0.31455		0.000000	0.000000
78	$PVC1^{\bullet}$(LUMO) / $PE^{\bullet}$(LUMO)	−0.08577	−0.05110	−0.03467		0.000000	0.000000
79	$PVC1^{\bullet}$(LUMO) / $PE^{\bullet}$(HOMO)	−0.08577	−0.20503	**0.11926**	**$PVC1^{\bullet}$(LUMO) → $PE^{\bullet}$(HOMO)**	**0.031250**	**−0.031250**
80	$PVC1^{\bullet}$(LUMO) / PE^{+}(LUMO)	−0.08577	−0.40480	**0.31903**	**$PVC1^{\bullet}$(LUMO) → PE^{+}(LUMO)**	**0.006875**	**−0.006875**
81	$PVC2^{\bullet}$(HOMO) / PE^{-}(LUMO)	−0.22663	0.22878	−0.45541		0.000000	0.000000
82	$PVC2^{\bullet}$(HOMO) / $PE^{\bullet}$(LUMO)	−0.22663	−0.05110	−0.17553		0.000000	0.000000
83	$PVC2^{\bullet}$(HOMO) / $PE^{\bullet}$(HOMO)	−0.22663	−0.20503	−0.02160		0.000000	0.000000
84	$PVC2^{\bullet}$(HOMO) / PE^{+}(LUMO)	−0.22663	−0.40480	**0.17817**	**$PVC2^{\bullet}$(HOMO) → PE^{+}(LUMO)**	**0.006875**	**−0.006875**
85	$PVC2^{\bullet}$(LUMO) / PE^{-}(LUMO)	−0.07229	0.22878	−0.30107		0.000000	0.000000
86	$PVC2^{\bullet}$(LUMO) / $PE^{\bullet}$(LUMO)	−0.07229	−0.05110	−0.02119		0.000000	0.000000
87	$PVC2^{\bullet}$(LUMO) / $PE^{\bullet}$(HOMO)	−0.07229	−0.20503	**0.13274**	**$PVC2^{\bullet}$(LUMO) → $PE^{\bullet}$(HOMO)**	**0.031250**	**−0.031250**
88	$PVC2^{\bullet}$(LUMO) / PE^{+}(LUMO)	−0.07229	−0.40480	**0.33251**	**$PVC2^{\bullet}$(LUMO) → PE^{+}(LUMO)**	**0.006875**	**−0.006875**
89	$PVC1^{+}$(HOMO) / PE^{-}(LUMO)	−0.47085	0.22878	−0.69963		0.000000	0.000000
90	$PVC1^{+}$(HOMO) / $PE^{\bullet}$(LUMO)	−0.47085	−0.05110	−0.41975		0.000000	0.000000
91	$PVC1^{+}$(HOMO) / $PE^{\bullet}$(HOMO)	−0.47085	−0.20503	−0.26582		0.000000	0.000000
92	$PVC1^{+}$(HOMO) / PE^{+}(LUMO)	−0.47085	−0.40480	−0.06605		0.000000	0.000000
93	$PVC2^{+}$(HOMO) / PE^{-}(LUMO)	−0.50460	0.22878	−0.73338		0.000000	0.000000
94	$PVC2^{+}$(HOMO) / $PE^{\bullet}$(LUMO)	−0.50460	−0.05110	−0.45350		0.000000	0.000000
95	$PVC2^{+}$(HOMO) / $PE^{\bullet}$(HOMO)	−0.50460	−0.20503	−0.29957		0.000000	0.000000
96	$PVC2^{+}$(HOMO) / PE^{+}(LUMO)	−0.50460	−0.40480	−0.09980		0.000000	0.000000

Table 8
Soft contacting between $PVC_{don,i}$ and $PTFE_{acc,i}$, $E_{PVCdon,i}$, $E_{PTFEacc,i}$, $\Delta E_{PVCdon,i/PTFEacc,i}$, $^{Fe}PVC_{don,i}$, $^{Fe}PTFE_{acc,i}$, $^{norm}TRfE_{PVCdon,i/PTFEacc,i}$, and $C^{norm}TRfE_{PVCdon,i/PTFEacc,i}$.

Path No.	Soft contacting between $PVC_{don,i}$ and $PTFE_{acc,i}$	$E_{PVCdon,i}$ [a.u.]	$E_{PTFEacc,i}$ [a.u.]	$\Delta E_{PVCdon,i/PTFEacc,i}$ [a.u.]	Feasible f-electron transfer pathway from $^{Fe}PVC_{don,i}$ to $^{Fe}PTFE_{acc,i}$	$^{norm}TRfE_{PVCdon,i/PTFEacc,i}$	$C^{norm}TRfE_{PVCdon,i/PTFEacc,i}$
97	$PVC1^{-}$(HOMO) / $PTFE^{-}$(LUMO)	0.06700	0.26369	−0.19669		0.00000	0.00000
98	$PVC1^{-}$(HOMO) / $PTFE^{\bullet}$(LUMO)	0.06700	−0.09374	**0.16074**	**$PVC1^{-}$(HOMO) → $PTFE^{\bullet}$(LUMO)**	**0.031250**	**−0.031250**
99	$PVC1^{-}$(HOMO) / $PTFE^{\bullet}$(HOMO)	0.06700	−0.24455	**0.31155**	**$PVC1^{-}$(HOMO) → $PTFE^{\bullet}$(HOMO)**	**0.031250**	**−0.031250**
100	$PVC1^{-}$(HOMO) / $PTFE^{+}$(LUMO)	0.06700	−0.45945	**0.52645**	$PVC1^{-}$**(HOMO) → $PTFE^{+}$(LUMO)**	**0.010625**	**−0.010625**
101	$PVC2^{-}$(HOMO) / $PTFE^{-}$(LUMO)	0.09314	0.26369	−0.17065		0.00000	0.00000
102	$PVC2^{-}$(HOMO) / $PTFE^{\bullet}$(LUMO)	0.09314	−0.09374	**0.18688**	**$PVC2^{-}$(HOMO) → $PTFE^{\bullet}$(LUMO)**	**0.031250**	**−0.031250**
103	$PVC2^{-}$(HOMO) / $PTFE^{\bullet}$(HOMO)	0.09314	−0.24455	**0.33769**	**$PVC2^{-}$(HOMO) → $PTFE^{\bullet}$(HOMO)**	**0.031250**	**−0.031250**
104	$PVC2^{-}$(HOMO) / $PTFE^{+}$(LUMO)	0.09314	−0.45945	**0.55259**	**$PVC2^{-}$(HOMO) → $PTFE^{+}$(HOMO)**	**0.010625**	**0.010625**
105	$PVC1^{\bullet}$(HOMO) / $PTFE^{-}$(LUMO)	−0.22376	0.26369	−0.48745		0.000000	0.000000
106	$PVC1^{\bullet}$(HOMO) / $PTFE^{\bullet}$(LUMO)	−0.22376	−0.09374	−0.13002		0.000000	0.000000
107	$PVC1^{\bullet}$(HOMO) / $PTFE^{\bullet}$(HOMO)	−0.22376	−0.24455	**0.33769**	**$PVC1^{\bullet}$(HOMO) → $PTFE^{\bullet}$(HOMO)**	**0.031250**	**−0.031250**
108	$PVC1^{\bullet}$(HOMO) / $PTFE^{+}$(LUMO)	−0.22376	−0.45945	**0.23569**	**$PVC1^{\bullet}$(HOMO) → $PTFE^{+}$(LUMO)**	**0.010625**	**−0.010625**
109	$PVC1^{\bullet}$(LUMO) / $PTFE^{-}$(LUMO)	−0.08577	0.26369	−0.34946		0.000000	0.000000
110	$PVC1^{\bullet}$(LUMO) / ($PTFE^{\bullet}$(LUMO)	−0.08577	−0.09374	**0.00797**	**$PVC1^{\bullet}$(LUMO) → $PTFE^{\bullet}$(LUMO)**	**0.031250**	**−0.031250**
111	$PVC1^{\bullet}$(LUMO) / $PTFE^{\bullet}$(HOMO)	−0.08577	−0.24455	**0.15878**	**$PVC1^{\bullet}$(LUMO) → $PTFE^{\bullet}$(HOMO)**	**0.03125**	**−0.03125**
112	$PVC1^{\bullet}$(LUMO) / $PTFE^{+}$(LUMO)	−0.08577	−0.45945	**0.37368**	**$PVC1^{\bullet}$(LUMO) → $PTFE^{+}$(LUMO)**	**0.010625**	**−0.010625**
113	$PVC2^{\bullet}$(HOMO) / $PTFE^{-}$(LUMO)	−0.22663	0.26369	−0.49032		0.000000	0.000000
114	$PVC2^{\bullet}$(HOMO) / $PTFE^{\bullet}$(LUMO)	−0.22663	−0.09374	−0.13289		0.000000	0.000000
115	$PVC2^{\bullet}$(HOMO) / $PTFE^{\bullet}$(HOMO)	−0.22663	−0.24455	**0.01792**	**$PVC2^{\bullet}$(HOMO) → $PTFE^{\bullet}$(HOMO)**	**0.031250**	**−0.031250**
116	$PVC2^{\bullet}$(HOMO) / $PTFE^{+}$(LUMO)	−0.22663	−0.45945	**0.23282**	**$PVC2^{\bullet}$(HOMO) → $PTFE^{+}$(LUMO)**	**0.010625**	**−0.010625**
117	$PVC2^{\bullet}$(LUMO) / $PTFE^{-}$(LUMO)	−0.07229	0.26369	−0.33598		0.000000	0.000000
118	$PVC2^{\bullet}$(LUMO) / $PTFE^{\bullet}$(LUMO)	−0.07229	−0.09374	**0.02145**	**$PVC2^{\bullet}$(LUMO) → $PTFE^{\bullet}$(LUMO)**	**0.031250**	**−0.031250**
119	$PVC2^{\bullet}$(LUMO) / $PTFE^{\bullet}$(HOMO)	−0.07229	−0.24455	**0.17226**	**$PVC2^{\bullet}$(LUMO) → $PTFE^{\bullet}$(HOMO)**	**0.031250**	**−0.031250**
120	$PVC2^{\bullet}$(LUMO) / $PTFE^{+}$(LUMO)	−0.07229	−0.45945	**0.38716**	**$PVC2^{\bullet}$(LUMO) → $PTFE^{+}$(LUMO)**	**0.010625**	**−0.010625**
121	$PVC1^{+}$(HOMO) / $PTFE^{-}$(LUMO)	−0.47085	0.26369	−0.73454		0.000000	0.000000
122	$PVC1^{+}$(HOMO) / $PTFE^{\bullet}$(LUMO)	−0.47085	−0.09374	−0.37711		0.000000	0.000000
123	$PVC1^{+}$(HOMO) / $PTFE^{\bullet}$(HOMO)	−0.47085	−0.24455	−0.22630		0.000000	0.000000
124	$PVC1^{+}$(HOMO) / $PTFE^{+}$(LUMO)	−0.47085	−0.45945	−0.01140		0.000000	0.000000
125	$PVC2^{+}$(HOMO) / $PTFE^{-}$(LUMO)	−0.50460	0.26369	−0.76829		0.000000	0.000000
126	$PVC2^{+}$(HOMO) / $PTFE^{\bullet}$(LUMO)	−0.50460	−0.09374	−0.41086		0.000000	0.000000
127	$PVC2^{+}$(HOMO) / $PTFE^{\bullet}$(HOMO)	−0.50460	−0.24455	−0.26005		0.000000	0.000000
128	$PVC2^{+}$(HOMO) / $PTFE^{+}$(LUMO)	−0.50460	−0.45945	−0.04515		0.000000	0.000000

Table 9
Soft contacting between $PTFE_{don,i}$ and $PVC_{acc,i}$, $E_{PTFEdon,i}$, $E_{PVCacc,i}$, $\Delta E_{PTFEdon,i/PVCacc,i}$, $^{Fe}PTFE_{don,i}$, $^{Fe}PVC_{acc,i}$, $^{norm}TRfE_{PTFEdon,i/PVCacc,i}$, and $C^{norm}TRfE_{PTFEdon,i/PVCacc,i}$.

Path No.	Soft contacting between $PTFE_{don,i}$ and $PVC_{acc,i}$	$E_{PTFEdon,i}$ [a.u.]	$E_{PVCacc,i}$ [a.u.]	$\Delta E_{PTFEdon,i/PVCacc,i}$ [a.u.]	Feasible f-electron transfer pathway from $^{Fe}PTFE_{don,I}$ to $^{Fe}PVC_{acc,i}$	$^{norm}TRfE_{PTFEdon,i/PVCacc,i}$	$C^{norm}TRfE_{PTFEdon,i/PVCacc,i}$
129	$PTFE^{-}$(HOMO) / $PVC1^{-}$(LUMO)	0.09858	0.19426	−0.09568		0.000000	0.000000
130	$PTFE^{-}$(HOMO) / $PVC2^{-}$(LUMO)	0.09858	0.21606	−0.11748		0.000000	0.000000
131	$PTFE^{-}$(HOMO) / $PVC1^{\bullet}$(LUMO)	0.09858	−0.08577	**0.18435**	**$PTFE^{-}$(HOMO) → $PVC1^{\bullet}$(LUMO)**	**0.010625**	**−0.010625**
132	$PTFE^{-}$(HOMO) / $PVC1^{\bullet}$(HOMO)	0.09858	−0.22376	**0.32234**	**$PTFE^{-}$(HOMO) → $PVC1^{\bullet}$(HOMO)**	**0.010625**	**−0.010625**
133	$PTFE^{-}$(HOMO) / $PVC2^{\bullet}$(LUMO)	0.09858	−0.07229	**0.17087**	**$PTFE^{-}$(HOMO) → $PVC2^{\bullet}$(LUMO)**	**0.010625**	**−0.010625**
134	$PTFE^{-}$(HOMO) / $PVC2^{\bullet}$(HOMO)	0.09858	−0.22663	**0.32521**	**$PTFE^{-}$(HOMO) → $PVC2^{\bullet}$(HOMO)**	**0.010625**	**−0.010625**
135	$PTFE^{-}$(HOMO) / $PVC1^{+}$(LUMO)	0.09858	−0.39067	**0.48925**	**$PTFE^{-}$(HOMO) → $PVC1^{+}$(LUMO)**	**0.010625**	**−0.010625**
136	$PTFE^{-}$(HOMO) / $PVC2^{+}$(LUMO)	0.09858	−0.41251	**0.51109**	**$PTFE^{-}$(HOMO) → $PVC2^{+}$(LUMO)**	**0.010625**	**−0.010625**
137	$PTFE^{\bullet}$(HOMO) / $PVC1^{-}$(LUMO)	−0.24455	0.19426	−0.43881		0.000000	0.000000
138	$PTFE^{\bullet}$(HOMO) / $PVC2^{-}$(LUMO)	−0.24455	0.21606	−0.46061		0.000000	0.000000
139	$PTFE^{\bullet}$(HOMO) / $PVC1^{\bullet}$(LUMO)	−0.24455	−0.08577	−0.15878		0.000000	0.000000
140	$PTFE^{\bullet}$(HOMO) / $PVC1^{\bullet}$(HOMO)	−0.24455	−0.22376	−0.02079		0.000000	0.000000
141	$PTFE^{\bullet}$(HOMO) / $PVC2^{\bullet}$(LUMO)	−0.24455	−0.07229	−0.17226		0.000000	0.000000
142	$PTFE^{\bullet}$(HOMO) / $PVC2^{\bullet}$(HOMO)	−0.24455	−0.22663	−0.01792		0.000000	0.000000
143	$PTFE^{\bullet}$(HOMO) / $PVC1^{+}$(LUMO)	−0.24455	−0.39067	**0.14612**	**$PTFE^{\bullet}$(HOMO) → $PVC1^{+}$(LUMO)**	**0.031250**	**−0.031250**
144	$PTFE^{\bullet}$(HOMO) / $PVC2^{+}$(LUMO)	−0.24455	−0.41251	**0.16796**	**$PTFE^{\bullet}$(HOMO) → $PVC2^{+}$(LUMO)**	**0.031250**	**−0.031250**
145	$PTFE^{\bullet}$(LUMO) / $PVC1^{-}$(LUMO)	−0.09374	0.19426	−0.28800		0.000000	0.000000
146	$PTFE^{\bullet}$(LUMO) / $PVC2^{-}$(LUMO)	−0.09374	0.21606	−0.30980		0.000000	0.000000
147	$PTFE^{\bullet}$(LUMO) / $PVC1^{\bullet}$(LUMO)	−0.09374	−0.08577	−0.00797		0.000000	0.000000
148	$PTFE^{\bullet}$(LUMO) / $PVC1^{\bullet}$(HOMO)	−0.09374	−0.22376	**0.13002**	**$PTFE^{\bullet}$(LUMO) → $PVC1^{\bullet}$(HOMO)**	**0.031250**	**−0.031250**
149	$PTFE^{\bullet}$(LUMO) / $PVC2^{\bullet}$(LUMO)	−0.09374	−0.07229	−0.02145		0.000000	0.000000
150	$PTFE^{\bullet}$(LUMO) / $PVC2^{\bullet}$(HOMO)	−0.09374	−0.22663	**0.13289**	**$PTFE^{\bullet}$(LUMO) → $PVC2^{\bullet}$(HOMO)**	**0.031250**	**−0.031250**
151	$PTFE^{\bullet}$(LUMO) / $PVC1^{+}$(LUMO)	−0.09374	−0.39067	**0.29693**	**$PTFE^{\bullet}$(LUMO) → $PVC1^{+}$(LUMO)**	**0.031250**	**−0.031250**
152	$PTFE^{\bullet}$(LUMO) / $PVC2^{+}$(LUMO)	−0.09374	−0.41251	**0.31877**	**$PTFE^{\bullet}$(LUMO) → $PVC2^{+}$(LUMO)**	**0.031250**	**−0.031250**
153	$PTFE^{+}$(HOMO) / $PVC1^{-}$(LUMO)	−0.61472	0.19426	−0.80898		0.000000	0.000000
154	$PTFE^{+}$(HOMO) / $PVC2^{-}$(LUMO)	−0.61472	0.21606	−0.83078		0.000000	0.000000
155	$PTFE^{+}$(HOMO) / $PVC1^{\bullet}$(LUMO)	−0.61472	−0.08577	−0.52895		0.000000	0.000000
156	$PTFE^{+}$(HOMO) / $PVC1^{\bullet}$(HOMO)	−0.61472	−0.22376	−0.39096		0.000000	0.000000
157	$PTFE^{+}$(HOMO) / $PVC2^{\bullet}$(LUMO)	−0.61472	−0.07229	−0.54243		0.000000	0.000000
158	$PTFE^{+}$(HOMO) / $PVC2^{\bullet}$(HOMO)	−0.61472	−0.22663	−0.38809		0.000000	0.000000
159	$PTFE^{+}$(HOMO) / $PVC1^{+}$(LUMO)	−0.61472	−0.39067	−0.22405		0.000000	0.000000
160	$PTFE^{+}$(HOMO) / $PVC2^{+}$(LUMO)	−0.61472	−0.41251	−0.20221		0.000000	0.000000

Therefore, $\Delta C^{Net.norm}TRfE$ (−0.12500) is obtained from the settings, where $E_{Av.whole,FePEdon,i}$ (−0.13486 a.u.) > $E_{Av.whole,FePVCacc,i}$ (−0.15582 a.u.).

We concluded that the PE surface comprising $^{whole,Fe}PE_{don,i}$ donated the *f-electrons* of $\Delta C^{Net.norm}TRfE$(−0.12500) to ^{whole,Fe}-$PVC^{acc,i}$ via the feasible *f-electron* transfer path ways in the settings, where $E_{Av.whole,FePEdon,i}$ (−0.13486 a.u.) > $E_{Av.whole,FePVCacc,i}$ (−0.15582 a.u.). Consequently, the PE surface resulted in the *positive net surface charge of PE* (*PE(+)*) with $^{Net.norm}SC_{soft,Av.PE}$(+0.12500). Although the PVC surface comprising $^{whole,Fe}PVC_{acc,i}$ accepts *f-electrons* of $\Delta C^{Net.norm}TRfE$(−0.12500), and results in *negative net surface charge of PVC* (*PVC(−)*) with $^{Net.norm}SC_{soft,Av.PVC}$(−0.12500).

3.2.3. ***Ce of PVC and PTFE*** *in a vacuum*

CE of PVC and PTFE were discussed based on the transfer of *f-electron* between $PVC_{ch.source,i}$ and $PTFE_{ch.source,i}$ in a vacuum.

First, we considered the hard contact between PVC and PTFE in a vacuum. $PVC_{ch.source,i}$ and $PTFE_{ch.source,i}$ were produced and anchored to the PVC and PTFE surfaces via hard contacting. Consequently, both surfaces exhibited charge-mosaic patterns comprising nano-regional charges that arose from $PVC_{ch.source,i}$ and $PTFE_{ch.source,i}$. Although the PVC and PTFE surfaces exhibited charge-mosaic patterns, $^{Total,norm}SC_{hard,PVCch.source,i}$ and ^{Total,norm}-$SC^{hard,PTFEch.source,i}$ were 0.00000 (neutral).

Second, we considered the soft contact between $PVC_{ch.source,i}$ and $PTFE_{ch.source,i}$ in a vacuum. A total of 64 possible contact combinations between $PVC_{ch.source,i}$ and $PTFE_{ch.source,i}$, which are divided into two categories, were considered. One category comprised 32 combinations of the *f-electron* transfer from $PVC_{don,i}$ and $PTFE_{acc,i}$, i.e., 32 pathways that might account for the *f-electron* transfer from $PVC_{don,i}$ to $PTFE_{acc,i}$, and the other category comprised 32 combinations of the *f-electron* transfer from $PTFE_{don,i}$ to $PVC_{acc,i}$, i.e., 32 pathways that might account for the *f-electron* transfer from $PTFE_{don,i}$ to $PVC_{acc,i}$. We assumed that $^{Total}I_{f\text{-}e,PVC}$ was identical to $^{Total}I_{f\text{-}e,PTFE}$, indicating that $^{norm}I_{PVCch.source,i}$ and $^{norm}I_{PTFEch.source,i}$ were normalized to the products by eight-time scissions.

First, we considered *f-electron* transfer from $PVC_{don,i}$ to $PTFE_{acc,i}$ in a vacuum.

All the combinations of the soft contacting of $PVC_{don,i}$ with $PTFE_{acc,i}$ are listed in Table 8 (Pathways 97–128). Although the total number of pathways were 32, we emphasized that $^{Fe}PVC_{don,i}$ could donate an *f-electron* to $^{Fe}PTFE_{acc,i}$ in settings where $\Delta E_{FePVCdon,i/FePTFEacc,i}$ > 0, i.e., $E_{FePVCdon,i}$ > $E_{FePTFEacc,i}$. Accordingly, each $^{norm}TRfE_{FePVdon,i/FePTFacc,i}$ was obtained in settings where $E_{FePVCdon,i}$ > $E_{FePTFEacc,i}$, i.e., where $^{norm}TRfE_{FePVdon,i/FePTFacc,i}$ was assigned to low $^{norm}I_{ch.source,i}$ compared with high $^{norm}I_{ch.source,i}$. The feasible *f-electron* transfer pathways are listed in Table 8 (Pathways 98, 99, 100, 102, 103, 104, 107, 108, 110, 111, 112, 115, 116, 118, 119, and 120). $PVC_{don,i}$, $PTFE_{acc,i}$, $E_{PVCdon,i}$, $E_{PTFEacc,i}$, $\Delta E_{FePVCdon,i/FePTFEacc,i}$, $^{Fe}PVC_{don,i}$, $^{Fe}PTFE_{acc,i}$, $^{norm}TRfE_{FePVCdon,i/FePTFEacc,i}$, and the $C^{norm}TRfE_{FePVCdon,i/FePTFEacc,i}$ are presented in Table 8 (Pathway numerals). Further, $^{Total,norm}TRfE_{FePVCdon,i/FePTFEacc,i}$ (0.37625) was obtained from the sum of $^{norm}TRfE_{FePVCdon,i/FePTFEacc,i}$s. $C^{Total,norm}$-$TRfE^{FePVCdon,i/FePTFEacc,i}$ (−0.37625) was the $^{Total,norm}TRfE_{FePVCdon,i/FePTFEacc,i}$ with charge sign.

Regarding these feasible *f-electron* transfer pathways, $C^{Total,norm}$-$TRfE^{FePVCdon,i/FePTFEacc,i}$ (−0.376250) is obtained via the *f-electron* transfer pathways of $^{Total}N_{FePVCdon,i/FePTFEacc,i}$ (16) in the settings where $\Delta^{Total}E_{FePVCdon,i/FePTFEacc,i}$ (3.70442 a.u.) = {$^{Total}E_{FePVCdon,i}$ (−0.89454 a.u.) − $^{Total}E_{FePTFEacc,i}$ (−4.59896 a.u.)} > 0.

We emphasized that the $C^{Total,norm}TRfE_{FePVCdon,i/FePTFEacc,i}$ (−0.37625) indicated the amount of the normalized transferred-*f-electron* from $^{Total,Fe}PVC_{don,i}$ to $^{Total,Fe}PTFE_{acc,i}$ via the $^{Total}N_{FePVCdon,i/FePTFEacc,i}$ (16) in settings where $^{Total}E_{FePVCdon,i}$ (−0.89454 a.u.) > $^{Total}E_{FePTFEacc,i}$ (−4.59896 a.u.).

Second, we considered *f-electron* transfer from $PTFE_{don,i}$ to $PVC_{acc,i}$ in a vacuum.

All the cases regarding the soft contacting of $PTFE_{don,i}$ with $PVC_{acc,i}$ are reported in Table 9 (Pathways 129–160). Although the total number of Pathways were 32, we emphasized that ^{Fe}-$PTFE_{don,i}$ could donate an *f-electron* to $^{Fe}PVC_{acc,i}$ in the settings where $\Delta E_{FePTFEdon,i/PVCacc,i}$ > 0, i.e., $E_{FePTFEdon,i}$ > $E_{FePVCacc,i}$. Accordingly, each $^{norm}TRfE_{FePTFEdon,i/FePVCacc,i}$ was obtained in the settings where $E_{FePTFEdon,i}$ > $E_{FePVCacc,i}$, i.e., those in which $^{norm}TRfE_{FePTFEdon,i/FePVCacc,i}$ was assigned to low $^{norm}I_{ch.source,i}$ as compared with high $^{norm}I_{ch.source,i}$. The feasible *f-electron* transfer pathways are presented in Table 9 (Pathways 131, 132, 133, 134, 135, 136, 143, 144, 148, 150, 151 and 152). $PTFE_{don,i}$, $PVC_{acc,i}$, $E_{PTFEdon,i}$, $E_{PVCacc,i}$, $\Delta E_{PTFEdon,i/PVCacc,i}$, $^{Fe}PTFE_{don,i}$, $^{Fe}PVC_{acc,i}$, $^{norm}TRfE_{FePTFEdon,i/FePVCacc,i}$, and $C^{norm}TRfE_{FePTFEdon,i/FePVCacc,i}$ are presented in Table 9 (Pathways numerals). Further, the $^{Total,norm}TRfE_{FePTFEdon,i/FePVCacc,i}$ (0.251250) was obtained from the sum of $^{norm}TRfE_{FePTFEdon,i/FePVCacc,i}$s. $C^{Total,norm}TRfE_{FePTFEdon,i/FePVCacc,i}$ (−0.251250) was the ^{Total,norm}-$TRfE^{FePTFEdon,i/FePVCacc,i}$ with charge sign.

Regarding these feasible *f-electron* transfer pathways, $C^{Total,norm}$-$TRfE^{FePTFEdon,i/FePVCacc,i}$ (−0.251250) is obtained via the *f-electron* transfer pathways of $^{Total,Fe}N_{FePTFEdon,i/FePVCacc,i}$ (12) in the settings where $\Delta^{Total}E_{FePTFEdon,i/FePVCacc,i}$ (3.19580 a.u.) = {$^{Total}E_{FePTFEdon,i}$ (−0.27258 a.u.) − $^{Total}EFe_{PVCacc,i}$ (−3.46838 a.u.)} > 0.

We emphasized that the $C^{Total,norm}TRfE_{FePTFEdon,i/FePVCacc,i}$ (−0.25125) indicated the amount of the normalized transferred-*f-electron* from $^{Total,Fe}PTFE_{don,i}$ to $^{Total,Fe}PVC_{acc,i}$ via the $^{Total}N_{FePTFEdon,i/FePVCacc,i}$ (12) in settings where $^{Total}E_{FePTFEdon,i}$ (−0.27258 a.u.) > $^{Total}E_{FePVCacc,i}$ (−3.46838 a.u.).

Next, after soft contacting, we speculated $^{Net.norm}SC_{soft,Av.PVC}$ and $^{Net.norm}SC_{soft,Av.PTFE}$ based on $C^{Total,norm}TRfE_{FePVCdon,i/FePTFEacc,i}$ (−0.37625) and $C^{Total,norm}TRfE_{FePTFEdon,i/FePVCacc,i}$ (−0.25125).

Regarding soft contacting, $\Delta C^{Net.norm}TRfE$ is given as $\Delta C^{Net.norm}$-$TRfE$(−0.12500) = $C^{Total,norm}TRfE_{FePVCdon,i/FePTFEacc,i}$ (−0.37625) - $C^{Total,norm}TRfE_{FePTFEdon,i/FePVCacc,i}$ (−0.25125). Accordingly, $\Delta C^{Net.norm}TRfE$ (−0.12500) is obtained via feasible *f-electron* transfer pathways in the settings where.

$$\begin{aligned}&\Delta^{Total}E(0.50862\ \text{a.u.})\\&= \Delta^{Total}E_{FePVCdon,i/FePTFEacc,i}\ (3.70442\ \text{a.u.}) - \Delta^{Total}E_{FePTFEdon,i/FePVCacc,i}\ (3.19580\ \text{a.u.})\\&= {}^{Total}E_{whole,FePVCdon,i}(-4.36292\text{a.u.}) - {}^{Total}E_{whole,FePTFEacc,i}(-4.87154\text{a.u.})\\&> 0\end{aligned} \tag{9}$$

By introducing $^{Total}N_{whole,FePVCdon,i}$ (28), and $^{Total}N_{whole,FePTFEacc,i}$ (28) into Eq. (9), the next equation would be obtained, as follows:

$$\begin{aligned}&= \{{}^{Total}E_{whole,FePVCdon,i}\ (-4.36292\ \text{a.u.})/\ {}^{Total}N_{whole,FePVCdon,i}\ (28)\}\\&\times {}^{Total}N_{whole,FePVCdon,i}\ (28) - \{{}^{Total}E_{whole,FePTFEacc,i}\ (-4.87154\ \text{a.u.})/\ {}^{Total}N_{whole,FePTFEacc,i}\ (28)\}\\&\times {}^{Total}N_{whole,FePTFEacc,i}\ (28).\end{aligned}$$

$$\begin{aligned}&= E_{Av.whole,FePVCdon,i}(-0.15582\text{a.u.})\times {}^{Total}N_{whole,FePVCdon,i}(28)\\&- E_{Av.whole,FePTFEacc,i}(-0.17398\text{a.u.})\times {}^{Total}N_{whole,FePTFEacc,i}(28)\\&> 0\end{aligned} \tag{10}$$

Therefore, $\Delta C^{Net.norm}TRfE$(−0.12500) is obtained in settings where $E_{Av.whole,FePVCdon,i}$ (−0.15582 a.u.) > $E_{Av.whole,FePTFEacc,i}$ (−0.17398 a.u.).

We concluded that the PVC surface comprising $^{whole,Fe}PVC_{don,i}$ donated *f-electrons* of $\Delta C^{Net.norm}TRfE$(−0.12500) to the ^{whole,Fe}-$PTFE^{acc,i}$ via the feasible *f-electron* transfer pathways in the settings where $E_{Av.whole,FePVCdon,i}$ (−0.15582 a.u.) > $E_{Av.whole,FePTFEacc,i}$ (−0.17398 a.u.). Consequently, the PVC surface results in *positive*

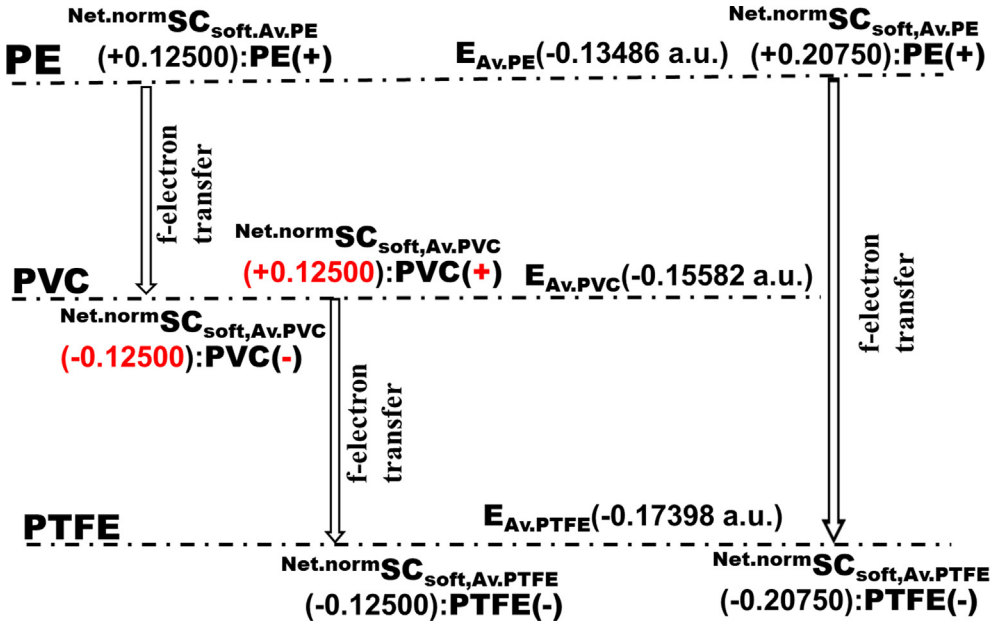

Fig. 4. Correlations of the net surface charges, average energy levels, and triboelectric series. Regarding the soft contact between PE and PVC, PE exhibited PE(+) with $^{Net.norm}SC_{soft.Av.PE}$(+0.12500), while PVC exhibited PVC(−) with $^{Net.norm}SC_{soft.Av.PVC}$(−0.12500) because EAv.PE(−0.13486 a.u.) > $E_{Av.\ PVC}$(−0.15582 a.u.). Conversely, regarding the soft contact between PVC and PTFE, PVC exhibited PVC(+) with $^{Net.norm}SC_{soft,Av.PVC}$(+0.12500) since $E_{Av.PVC}$(−0.15582 a.u.) > $E_{Av.\ PTFEacc,i}$ (−0.17398 a.u.). These results indicated that the net surface charge depended on the average energy level of the *naked-activated-charge-sources*. The alignment of EAv.PE(−0.13486 a.u.)-$E_{Av.PVC}$(−0.15582 a.u.)-$E_{Av.\ PTFE}$(−0.17398 a.u.) is identical to the alignment from positive to negative charge sign on the triboelectric series for PE-PVC-PTFE.

net surface charge of PVC (*PVC(+)*) with $^{Net.norm}SC_{soft,Av.\ PVC}$(+0.12500). Although the PTFE surface comprising ^{whole,Fe}-$PTFE^{acc,i}$ accepts *f-electrons* of $\Delta C^{Net.norm}TRfE$(−0.12500), and results in *negative net surface charge of PTFE* (*PTFE*(−)) with $^{Net.norm}SC_{soft,Av.\ PTFE}$(−0.12500).

3.2.4. Correlations among the charge signs, average energy levels and triboelectric series

We focused on the surface charge of PVC that was induced via contact with PE or PTFE.

Firstly, regarding CE between PE and PVC in a vacuum, we concluded that the PE surface comprising $^{whole,Fe}PE_{don,i}$ donated the *f-electrons* of $\Delta C^{Net.norm}TRfE$(−0.12500) to $^{whole,Fe}PVC_{acc,i}$ via the feasible *f-electron* transfer path ways in settings where $E_{Av.whole,FePEdon,i}$ (−0.13486 a.u.) > $E_{Av.whole,FePVCacc,i}$ (−0.15582 a.u.). Thus, the PE surface yielded PE(+) with $^{Net.norm}SC_{soft,Av.PE}$ (+0.12500), while the PVC surface comprising $^{whole,Fe}PVC_{acc,i}$ accepted the *f-electrons* of $\Delta C^{Net.norm}TRfE$ (−0.12500), yielding PVC(−) with $^{Net.norm}SC_{soft,Av.PVC}$ (−0.12500).

Second, we concluded that the PVC surface comprising ^{whole,Fe}-$PVC^{don,i}$ donated the *f-electrons* of $\Delta C^{Net.norm}TRfE$ (−0.12500) to the $^{whole,Fe}PTFE_{acc,i}$, via the feasible *f-electron* transfer pathways in settings where $E_{Av.whole,FePVCdon,i}$ (−0.15582 a.u.) > $E_{Av.whole,FePTFEacc,i}$ (−0.17398 a.u.). Consequently, the PVC surface comprising ^{whole,Fe}-$PVC^{don,i}$ resulted in PVC(+) with $^{Net.norm}SC_{soft,Av.PVC}$(+0.12500). Conversely, the PTFE surface comprising $^{whole,Fe}PTFE_{acc,i}$ accepted the *f-electrons* of $\Delta C^{Net.norm}TRfE$(−0.12500) to yield PTFE(−) with $^{Net.norm}SC_{soft,Av.PTFE}$(−0.12500).

Regarding the soft contact between PE and PVC, PVC exhibited PVC(−) with $^{Net.norm}SC_{soft,Av.PVC}$ (−0.12500) because $E_{Av.whole,FePEdon,i}$ (−0.13486 a.u.) > $E_{Av.whole,FePVCacc,i}$ (−0.15582 a.u.). Conversely, in the soft contact between PVC and PTFE, PVC exhibited PVC(+) with $^{Net.norm}SC_{soft,Av.PVC}$(+0.12500) because $E_{Av.whole,FePVCdon,i}$ (−0.15582 a.u.) > $E_{Av.whole,FePTFEacc,i}$ (−0.17398 a.u.), indicating the net surface charge depended on the average energy level of the *naked-activated-charge-sources* (Fig. 4).

Conversely, by aligning PE, PVC, and PTFE to their average energy levels, the alignment of PE(EAv.PE; −0.13486 a.u.)-PVC ($E_{Av.PVC}$; −0.15582 a.u.)-PTFE($E_{Av.PTFE}$; −0.17398 a.u.) was identical to the alignment from the positive to negative charge signs on the triboelectric series [28], indicating that the triboelectric series might be aligned to the polymer exhibiting high to low average energy levels.

4. Conclusions

Since CE is accompanied by polymer destruction, we assumed that it is also accompanied by covalent bond scission, which is induced by the "hard contacting" of polymers in a vacuum. *Naked-activated-mechano-anions* and *naked-activated-mechano-cations*, which are produced by the heterogeneous covalent bond scission of the polymer main chain, and the *naked-activated-mechano-radicals*, which are produced by the homogeneous covalent bond scission of the polymer main chain, accounted for the charge sources. Moreover, these charge sources were anchored to the polymer surface and isolated on the surface in a vacuum. Thus, such a polymer surface exhibited a non-uniform charge pattern comprising a nano-scale charge region that was obtained from the charge sources. Although the surface exhibited a non-uniform charge pattern, the net charge was neutral. Sequentially, owing to "soft contacting," which does not induce covalent bond scission, the transfer of an *f-electron* from the charge sources as the donor to another charging source as the acceptor via feasible electron transfer pathways was accomplished via settings where the energy level of the charge source (donor) was higher than that the acceptor one, wherein the activation energy of the transfer of the *f-electron* was expected to be zero. A net surface charge was obtained employing a setting in which the average energy level of the charge sources as the donor is higher than that as acceptors. Consequently, the surface comprising the charge sources with a high average energy level exhibited positive net surface charge. However, another

surface comprising charge sources with a low average energy level exhibited a negative net surface charge.

We concluded thus: 1. The charge sources were *naked-activated-mechano-anions*, *naked-activated-mechano-cations* and *naked-activated-mechano-radicals*, which were anchored and isolated on the surface in a vacuum. 2. An *f-electron* acted as the charge carrier. 3. The net surface charge was obtained via *f-electron* transfer from the donor charge sources exhibiting a high average energy level to the acceptor charge sources exhibiting a low average energy level. Consequently, the surfaces comprising the donors and acceptors exhibited positive and negative net surface charges, respectively. 4. The net surface charge depended on the average energy level of the charge sources. 5. The alignment of PE(EAv.PE; −0.13486 a.u.)-PVC($E_{Av.PVC}$; −0.15582 a.u.)-PTFE ($E_{Av.PTFE}$; −0.17398 a.u.) was identical to the alignment from the positive to negative charge signs on the triboelectric series [28]. The triboelectric series might be aligned to a polymer exhibiting high to low average energy levels.

Declaration of Competing Interest

The authors declare that they have no known competing financial interests or personal relationships that could have appeared to influence the work reported in this paper.

References

[1] H.T. Baytekin, A.Z. Patashinski, M. Branicki, B. Baytekin, S. Soh, B.A. Grzybowski, The mosaic of surface charge in contact electrification, Science 333 (2011) 308–312.

[2] H.T. Baytekin, B. Baytekin, J.T. Incorvati, B.A. Grzybowski, Material transfer and polarity reversal in contact charging, Angew. Chem. Int. Ed. 51 (2012) 4843–4847.

[3] T.A.L. Burgo, T.R.D. Ducati, K.R. Francisco, K.J. Clinckspoor, F. Galembeck, S.E. Galembeck, Triboelectricity: Macroscopic charge patterns formed by self-arraying ions on polymer surfaces, Langmuir 28 (2012) 7407–7416.

[4] F. Galembeck, T.A.L. Burgo, L.B.S. Balestrin, R.F. Gouveia, C.A. Silva, A. Galembeck, Friction, tribochemistry and triboelectricity: Recent progress and perspectives, RSC Adv. 4 (109) (2014) 64280–64298.

[5] R.K. Pandey, H. Kakehashi, H. Nakanishi, S. Soh, Correlating material transfer and charge transfer in contact electrification, J. Phys. Chem. C 122 (2018) 16154–16160.

[6] J. Zhang, M.L. Coote, S. Ciampi, Electrostatics and electrochemistry: Mechanism and scope of charge-transfer reactions on the surface of tribocharged insulators, J. Am. Chem. Soc. 143 (2021) 3019–3032.

[7] M. Sakaguchi, J. Sohma, ESR evidence for main-chain scission produced by mechanical fracture of polymers at low temperature, J. Polym. Sci. Polym. Phys. Ed. 13 (1975) 1233–1245.

[8] M. Sakaguchi, T. Yamaguchi, S. Shimada, Y. Hori, ESR study on molecular motion of chain end radicals of polyethylene molecules anchored on fresh surfaces of polyethylene and polytetrafluoroethylene, Macromolecules 26 (1993) 2612–2615.

[9] M. Sakaguchi, S. Shimada, Y. Hori, A. Suzuki, F. Kawaizumi, M. Sakai, S. Bandow, Molecular motion of polyethylene chain-end radicals tethered on the surface of poly(tetrafluoroethy1ene) in vacuo at extremely low temperatures, Macromolecules 28 (1995) 8450–8452.

[10] M. Sakaguchi, S. Shimada, K. Yamamoto, M. Sakai, Site exchange motion of ends of isolated single polyethylene chains tethered on the poly (tetrafluoroethylene) surface in a vacuum at 2.6 K, Macromolecules 30 (1997) 8521–8523.

[11] M. Sakaguchi, T. Ohura, T. Iwata, S. Takahashi, S. Akai, T. Kan, H. Murai, M. Fujiwara, O. Watanabe, M. Narita, Diblock copolymer of bacterial cellulose and poly(methyl methacrylate) initiated by chain-end-type radicals produced by mechanical scission of glycosidic linkages of bacterial cellulose, Biomacromolecules 11 (2010) 3059–3066.

[12] M. Sakaguchi, T. Ohura, T. Iwata, Y. Enomoto-Rogers, Nano cellulose particles covered with block copolymer of cellulose and methyl methacrylate produced by solid mechano chemical polymerization, Polym. Degrad. Stab. 97 (2012) 257–263.

[13] T. Motokawa, M. Makino, M. Sakaguchi, Peroxy radicals as motional probes at the end of isolated polystyrene chains on the cellulose surfaces in a vacuum, Cellulose 23 (2016) 1123–1135.

[14] M. Sakaguchi, H. Kinpara, Y. Hori, S. Shimada, H. Kashiwabara, Ionic products from the mechanical fracture of solid polypropylene, Polymer 25 (1984) 944–946.

[15] M. Sakaguchi, H. Kinpara, Y. Hori, S. Shimada, H. Kashiwabara, Ionic species produced by mechanical fracture of solid polymer. III. Anions from polytetrafluoroethylene, J. Polym. Sci. Polym. Phys. Ed. 25 (1987) 1431–1437.

[16] M. Sakaguchi, H. Kinpara, Y. Hori, S. Shimada, H. Kashiwabara, Ionic products in ground polymer. IV. Anions in poly(vinylidene fluoride), J. Polym. Sci. Part B Polym. Phys. 26 (1988) 1307–1312.

[17] M. Sakaguchi, Y. Miwa, S. Hara, Y. Sugino, K. Yamamoto, S. Shimada, Triboelectricity in polymers: Effects of the ionic nature of carbon-carbon bonds in the polymer main chain on charge due to yield of mechanoanions produced by heterogeneous scission of the carbon-carbon bond by mechanical fracture, J. Electrostat. 62 (2004) 35–50.

[18] M. Sakaguchi, M. Makino, T. Ohura, T. Iwata, Mechanoanions produced by mechanical fracture of bacterial cellulose: ionic nature of glycosidic linkage and electrostatic charging, J. Phys. Chem. A. 116 (2012) 9872–9877.

[19] M. Sakaguchi, M. Makino, T. Ohura, T. Iwata, The Correlation between the ionic degree of covalent bond comprising polymer main chain and the ionic yield due to mechanical fracture, Polymer 55 (2014) 1917–1919.

[20] M. Sakaguchi, H. Kinpara, Y. Hori, S. Shimada, H. Kashiwabara, Mechano ions produced by mechanical fracture of solid polymer. **5.** Cationic polymerization of isobutyl vinyl ether initiated by the mechano cation of poly(viny1idene fluoride), Macromolecules 22 (1989) 1277–1280.

[21] Gaussian 09, Revision **E.01**, M. J. Frisch, et al. Gaussian, Inc., Wallingford CT, **2009.**

[22] A.D. Becke, Density-functional thermochemistry. III. The role of exact exchange, J. Chem. Phys. 98 (1993) 5648–5652.

[23] R. Dennington, T. Keith, J. Millam, GaussView, Version 5, Semichem Inc., Shawnee Mission, KS, 2009.

[24] X. Li, M.J. Frisch, Energy-represented direct inversion in the iterative subspace within a hybrid geometry optimization method, J. Chem. Theory Comput. 2 (2006) 835–839.

[25] M. Sakaguchi, S. Shimada, H. Kashiwabara, Mechanoions produced by mechanical fracture of solid polymer. 6. A generation mechanism of triboelectricity due to the reaction of mechanoradicals with mechano anions on the friction surface, Macromolecules 23 (1990) 5038–5040.

[26] M. Sakaguchi, M. Makino, T. Ohura, T. Iwata, Contact electrification of polymers due to electron transfer among mechano anions, mechano cations and mechano radicals, J. Electrostat. 72 (2014) 412–416.

[27] Y. Fang, S. Gonuguntla, S. Soh, Universal nature-inspired coatings for preparing noncharging surfaces, ACS Appl. Mater. Interfaces 9 (2017) 32220–32226.

[28] J. Henniker, Triboelectricity in polymers, Nature 196 (1962) 474.